

Electronic Theses and Dissertations, 2004-2019

2011

Ultra High Density Spectral Beam Combining By Thermal Tuning Of Volume Bragg Gratings In Photo-thermo-refractive Glass

Derrek Drachenberg
University of Central Florida

 Part of the [Electromagnetics and Photonics Commons](#), and the [Optics Commons](#)
Find similar works at: <https://stars.library.ucf.edu/etd>
University of Central Florida Libraries <http://library.ucf.edu>

This Doctoral Dissertation (Open Access) is brought to you for free and open access by STARS. It has been accepted for inclusion in Electronic Theses and Dissertations, 2004-2019 by an authorized administrator of STARS. For more information, please contact STARS@ucf.edu.

STARS Citation

Drachenberg, Derrek, "Ultra High Density Spectral Beam Combining By Thermal Tuning Of Volume Bragg Gratings In Photo-thermo-refractive Glass" (2011). *Electronic Theses and Dissertations, 2004-2019*. 1844. <https://stars.library.ucf.edu/etd/1844>

**ULTRA HIGH DENSITY SPECTRAL BEAM COMBINING BY THERMAL
TUNING OF VOLUME BRAGG GRATINGS IN PHOTO-THERMO-
REFRACTIVE GLASS**

by

DERREK DRACHENBERG

M.S. Optics, University of Central Florida, 2009

B.S.E.E., University of Central Florida, 2007

A Dissertation submitted in partial fulfillment of the requirements
for the degree of Doctor of Philosophy
in CREOL, the College of Optics and Photonics
at the University of Central Florida
Orlando, Florida

Fall Term
2011

Major Professor: Leonid Glebov

© 2011 Derrek Reginald Drachenberg

ABSTRACT

High power lasers with diffraction limited beam quality are desired for many applications in defense and manufacturing. A lot of applications require laser beams at the 100 kW power level along with divergence close to the diffraction limit. The figure of merit for a beam used in such applications should be radiance which determines the laser power delivered to a remote target. One of the primary limiting factors is thermal distortion of a laser beam caused by excessive heat generated in the laser media. Combination of multiple laser beams is usually considered as a method to mitigate these limitations. Spectral beam combining (SBC) by volume Bragg gratings (VBGs) is a very promising method for the future of high radiance lasers that needs to achieve 100 kW-level power. This work is dedicated to development of methods to increase spectral density of combined beams keeping their divergence at an acceptably low level.

A new figure of merit for a beam combining system is proposed, the Beam Combining Factor (BCF), which makes it possible to distinguish the quality of the individual beams from the quality of beam combining. Also presented is a method of including the effect of beam divergence and spectral bandwidth on the performance of VBGs, as well as a method to optimize VBG parameters in terms of thickness and refractive index modulation for an arbitrary number of beams.

A novel thermal tuning technique and apparatus is presented with which the SBC system can be tuned for peak efficiency from low to high power without the need for mechanical re-

alignment. Finally, a thermally tuned SBC system with five beams, with a spectral separation between beams of 0.25 nm at a total power of 685 W is presented. The results show the highest power spectral density and highest spectral radiance of any SBC system to date. Recent demonstrations in SBC by multiplexed VBGs and the use of super Gaussian beams for beam quality improvement are also discussed.

ACKNOWLEDGEMENTS

I would like to thank the Directed Energy Professional Society (DEPS) for the DEPS Graduate Directed Energy Scholarship in High Energy Lasers for 2008, 2009, and 2010. I would also like to thank the Defense Advanced Research Projects Agency (DARPA), and the Air Force Research Lab (AFRL) for partial funding of the research in this dissertation.

TABLE OF CONTENTS

LIST OF FIGURES	VIII
LIST OF TABLES.....	XIV
1 INTRODUCTION	1
1.1 Survey of Coherent Beam Combining	2
1.2 Survey of Spectral Beam Combining	7
1.2.1 Spectral Beam Combining by Angularly Dispersive Elements	8
1.2.2 Spectral Beam Combining by Frequency Selective Filters (VBGs)	18
2 RADIANCE (BRIGHTNESS) AND THE BEAM COMBINING FACTOR (BCF)	27
2.1 Radiance (Brightness) Defined.....	27
2.2 Beam Combining Factor (BCF)	28
3 MODELING VBGs FOR HIGH DENSITY SBC.....	30
3.1 Coupled Wave Theory for Thick Holograms	31
3.2 Modeling Beam Divergence and Spectral Bandwidth Effects in VBGs	35
3.2.1 Introduction to the Effect of Non-Ideal Beams on VBG performance	35
3.2.2 Formal Approach to Including Non-Ideal Beam Effects in the VBG Model.....	36
3.2.3 Computational Implementation of Simultaneous Angle and Wavelength Convolutions.....	38
3.2.4 Experimental Verification of Beam Divergence, and Bandwidth Effects on VBG Performance	41
4 OPTIMIZATION OF VBG PARAMETERS FOR SBC	43
4.1 Single Stage Optimization.....	43
4.2 N-Stage Optimization.....	53
5 MODELING THE BEAM QUALITY OF COMBINED GAUSSIAN BEAMS:	58
5.1 Modeling the Combined M^2 of Ideal Gaussian Beams with Beam Waist Mismatch	58
5.2 Ideal Alignment of Non-Ideal Beams, $M^2 \neq 1$	65
5.3 Experimental Setup for Beam Waist Measurement of Spectrally Combined Beams	67
6 THERMAL TUNING OF VOLUME BRAGG GRATINGS	70
7 TESTING OF VOLUME BRAGG GRATINGS FOR HIGH POWER SPECTRAL BEAM COMBINING ...	82
7.1 Testing Diffraction Efficiency and Absolute Losses.....	82
7.2 Testing for Beam Quality, Astigmatism and Defocus of a Diffracted Beam	86
8 HIGH POWER SBC OF FIBER LASERS WITH ULTRA HIGH SPECTRAL DENSITY.....	89
8.1 Two Beam Experiments	89
8.2 Five Beam Experiments	92

8.2.1	Ultra High Density SBC with Low Power Beams	92
8.2.2	Ultra High Density, High Power SBC with High Absorption VBGs	94
8.2.3	Ultra High Density, High Power SBC with Low Absorption VBGs	96
8.3	Wavelength, and Pointing Stability of Lasers	100
9	FUTURE DIRECTIONS FOR RESEARCH IN VBG-BASED SBC.....	104
9.1	Spectral Beam Combining by Multiplexed Volume Bragg Gratings	104
9.2	Beam Quality Improvement with Flat Top Heating Profile	107
10	CONCLUSIONS.....	112
	LIST OF REFERENCES.....	116

LIST OF FIGURES

Figure 1: Coherent Beam Combining by Active Feedback ¹	3
Figure 2: Self Organized Coherent Beam Combining ¹	5
Figure 3: The predicted mean values of the addition efficiency (filled circles) and effective reflectivity (open circles) as functions of the number of array elements. The experimental results are plotted with squares. ¹¹	5
Figure 4: Multiplexed Volume Bragg Grating as 1x2 splitter/combiner ¹²	6
Figure 5: Passive Coherent Beam Combining by Multiplexed Volume Bragg Gratings ¹²	7
Figure 6: SBC by a transmitting ³⁴ (left) or reflecting ¹ (right) surface diffraction grating.....	9
Figure 7: Diffraction grating. Littrow condition occurs for $\theta = 0$ (the 1 st diffracted order overlaps with the incident beam)	11
Figure 8: Laser wavelength tuning by gratings used in the Littrow condition for high ⁶⁹ (left) and low ⁷⁰ (right) diffraction efficiency configurations.....	12
Figure 9: SBC by diffraction grating in “Littrow configuration”. A single channel is highlighted and consists of a seed source (1), a first (2) and second pre-amplifier (3), the main amplifier (4), the folding mirrors (5) and the grating (6). ³⁹	14
Figure 10: SBC by dual diffraction gratings for beam quality improvement and relaxing of fiber laser bandwidth requirements ³⁶	16
Figure 11: Propagation of optical rays through a volume Bragg grating. <i>Nf</i> and <i>Nf,ex</i> – normals to the front surface for incident (<i>li</i>) and diffracted (<i>ld</i>) beams; <i>Kim</i> and <i>Kdm</i> – wave	

<p>vectors of incident and diffracted beams inside the grating medium; KG - grating vector; ϕ – grating inclination; θ_i and θ_d – angles of incidence and diffraction; θ_m –Bragg angle; θ_m^* – incident Bragg angle.⁵⁰</p>	19
<p>Figure 12: Possible orders of Bragg diffraction inside medium. l_i and l_d –incident and diffracted beams; Ki – wave vector of incident beam; KG –grating vector; θ_m – Bragg angle; θ_m^* – incident Bragg angle.⁵⁰</p>	20
<p>Figure 13: Reflecting volume Bragg grating spectrum for SBC.⁶¹</p>	21
<p>Figure 14: Self organized spectral beam combining by volume Bragg gratings in a common cavity⁵⁶</p>	23
<p>Figure 15: Architecture for five channel SBC by reflecting VBGs.....</p>	24
<p>Figure 16: Monolithic SBC module⁶⁰</p>	25
<p>Figure 17: SBC system with stack of five monolithic beam combiners⁶⁰</p>	25
<p>Figure 18: Modeling of VBG diffraction efficiency versus detuning from Bragg wavelength....</p>	31
<p>Figure 19: Numerical convolution in angle space</p>	39
<p>Figure 20: Numerical convolution in wavelength space.....</p>	40
<p>Figure 21: Comparison Theory(dash) v.s. Experiment (solid); VBG refractive index modulation = 102.5 ppm, Bragg Period = 531.81 nm, thickness = 3.99 mm; Laser spectral bandwidth = 0.144 nm, divergence = diffraction limited.</p>	41

Figure 22: Comparison Theory(dash) v.s. Experiment (solid); VBG refractive index modulation = 415 ppm, thickness = 3.5 mm, Bragg Period = 1066.57 nm; Laser spectral bandwidth < 20 pm, divergence = 23 mrad (full width)	42
Figure 23: Diffraction efficiency spectrum for plane wave, and 0.5 mrad (half angle) divergent beam	45
Figure 24: Combining efficiency, single stage SBC, 2 beams, 0.25 nm separation, 0.5 mrad div (half angle)	47
Figure 25: Software interface for VBG optimization	48
Figure 26: Illustration of iterative SBC system optimization	55
Figure 27: Efficiency of 5-channel SBC as a function of VBG thickness and refractive index modulation	56
Figure 28: Diffraction efficiency spectra of VBGs for an optimized system	57
Figure 29: Beam radius v.s. propagation distance for two beams with a divergence difference of 0.100 mrad	59
Figure 30: Cross section of two beams with 0.100 mrad divergence difference after 10 m propagation	60
Figure 31: Relative Radiance in a combined beam v.s. M^2 for individual beams.....	63
Figure 32: Beam radius v.s. propagation distance for five beams with a total divergence difference of 0.100 mrad.....	64

Figure 33: Cross section of five beams with 0.100 mrad total divergence difference after 10 m propagation	64
Figure 34: Demultiplexing and beam measurement experimental setup.....	69
Figure 35: VBG thermal tuning apparatus.....	70
Figure 36: The tail of a diffraction efficiency spectrum illustrating sensitivity of losses for a transmitting beam to offset of wavelength.....	72
Figure 37: Temperature stability of TEC while controlling a VBG. At the 70 °C set point the average temperature was 68.7 °C, and the standard deviation was 1.0 °C.	73
Figure 38: Experimental setup for diffraction efficiency spectra measurement in VBGs exposed to high power laser radiation.....	75
Figure 39: Diffraction efficiency under various heating conditions	76
Figure 40: Bragg wavelength profile across the aperture under various heating conditions.....	78
Figure 41: Profiles of deviation from initial Bragg wavelength for external heating to 70°C and a combination of external heating to 55°C and 160 W laser radiation.....	79
Figure 42: Relative diffraction efficiency test setup.....	84
Figure 43: Absolute efficiency and loss test setup.....	85
Figure 44: Typical result from absolute efficiency and loss measurement	85
Figure 45: Two channel high power SBC experimental setup	90
Figure 46: Two channel beam combining efficiency at different power levels and VBG edge temperatures	90

Figure 47: 2-Beam, 300 W, SBC M^2	91
Figure 48: Five channel, combined low power beam quality, $M^2=1.06$	92
Figure 49: Quality of a combined beam in the five beam 100 W SBC system, 20 W each beam.	94
Figure 50: Combined beam quality of the five beam 750 W SBC system using interim VBGs..	95
Figure 51: Thermo image of last VBG from lower absorption VBG set in the five beam 750 W spectral combiner.	99
Figure 52: Photo of experimental setup with beam propagating from right to left.	99
Figure 53: Combined spectrum of 750 W SBC system.....	100
Figure 54: Combined beam quality of the five beam 750 W SBC system using final low absorption VBGs.....	100
Figure 55: Long term wavelength stability of high power fiber lasers.....	101
Figure 56: Long term (1hr 45min) pointing stability of high power fiber lasers after 50 mm lens. Standard deviation in focal position = 0.62 μm , which translates to 12.4 μrad in angle. The half-angle diffraction limited divergence for the 6 mm diameter beam is 112 μrad	103
Figure 57: Long term (1hr 45min) points in the bucket curve based on the data from Figure 56. The plot shows the ratio of points (vertical-axis) that fall within a given radius (horizontal-axis).....	103
Figure 58: Multiplexed spectral beam combining geometry ⁷⁹	105

Figure 59: Combined M^2 for SBC of two beams by multiplexed VBGs..... 106

Figure 60: Calculated M^2 for Gaussian (dashed line) and super Gaussian (solid line) high power beams transmitting through as a function of phase shift where phase shift is proportional to incident laser power at glass absorption⁸⁰ 108

Figure 61: Experimental setup to measure M^2 for Gaussian (without pi-shaper) and super Gaussian (with pi-shaper) high power laser beams. 109

Figure 62: Measured M^2 for Gaussian (Circles) and super Gaussian (Diamonds) high power beams transmitting through high absorption PTR glass as a function of normalized incident laser power. 110

LIST OF TABLES

Table 1: Summary of beam propagation factor, divergence, Rayleigh length, and radiance findings for two and five beam spectral beam combining.....	67
Table 2: Diffraction efficiency and M^2 under various heating conditions.....	80
Table 3: Summary of VBG properties	97

1 INTRODUCTION

High power lasers with diffraction limited beam quality are desired for many applications in defense and manufacturing. For applications in which the beam must propagate for a distance, higher power is only beneficial if diffraction limited beam quality is maintained. The figure of merit for a beam used in such applications should be radiance or brightness which are considered here to be interchangeable. Radiance is defined as the power divided by the product of the solid angle in the far field and the unit area in the beam waist. The radiance for a radially symmetric Gaussian beam is given in Equation 1 below ¹.

$$B = \frac{P}{\lambda^2 * (M^2)^2} \quad (1)$$

Solid state and gas lasers have been the most successful at achieving high power with a single gain element, but each has its drawbacks. Gas lasers require large quantities of toxic materials, and solid state rod lasers tend to have diminishing returns in radiance as power is increased due to thermal distortions². Thin disk, slab, and fiber lasers attempt to overcome these thermal limitations with unique geometries². Fiber lasers with diffraction limited beam quality have recently achieved powers of a few kW ², and are excellent candidates for high radiance applications. Ultimately, the radiance of single aperture lasers, whether it be gas, solid state, or fiber, will be limited by non-linear and thermal effects in the active medium. Theoretical modeling has predicted that high power limits on diffraction limited fiber lasers are 10 kW to 36 kW for broadband and 2 kW for narrow band lasers ³.

A major goal of high radiance beams has been to reach 100 kW of diffraction limited power for short and mid ranged defense applications. It is probable that to reach such power levels, beam combining will be required. If radiance is not a concern, beams can be combined by arranging side by side arrays of beams which can be manipulated to produce any configuration desired. This method, however, cannot increase the radiance according to the radiance theorem. The two important theorems that relate to radiance in an optical system are as follows. The radiance of the light distribution produced by a passive imaging system cannot be greater than the original source radiance, and the radiance of a collection of mutually incoherent, but otherwise identical, sources cannot be increased by a passive linear optical system to a level greater than the radiance of the single brightest source⁴. High radiance beam combining efforts can be broken up into two main categories, coherent, and incoherent beam combining. The focus of this paper is on incoherent, spectral beam combining (SBC), but coherent beam combining (CBC) will be discussed only in as much detail as is required to compare it to SBC.

1.1 Survey of Coherent Beam Combining

First used in longer wavelength regions of the spectrum, CBC was first used in the form of a phased array of emitters for radar and radio wave beam direction⁵. It then moved into the optical range as a method to steer and combine individual stripes of a semiconductor laser⁶. Many different methods of CBC have been demonstrated such as common resonator, evanescent wave, self-organized, active feedback, and nonlinear optical¹. The most successful method for

high radiance applications has been CBC by active feedback phase control of an array of gain elements and has had significant progress recently.

Figure 1 illustrates the operation of CBC of multiple apertures with active feedback. Radiation from a seed laser is first split into multiple beams each of which is introduced to gain elements at the amplification stage. The phase of the beam after each amplification stage is compared to the phase of the seed laser. Feedback is then sent to phase modulators that modify the phase in each beam before the amplification stage. When properly implemented, the beams interfere constructively in the far field producing a near diffraction limited beam.

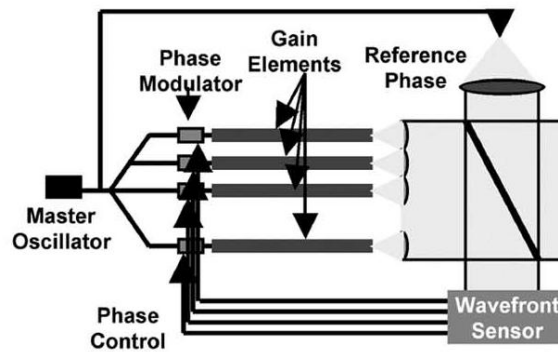


Figure 1: Coherent Beam Combining by Active Feedback¹

This method, as employed by Northrup Grumman for the Joint High Power Solid State Laser (JHPSSL) project⁷, claims the highest power solid state laser to date, with 105 kW of

output power from five diode pumped ceramic slab lasers, and decent far field beam quality with $M^2 = 3.00$. Total efficiency is around 20 %, and along with beam quality is a major area for future improvement. If beam quality is improved, this would be the highest radiance solid state source available. As of now, the radiance is close to that of a diffraction limited 10 kW laser. Coherent beam combining with active feedback has clear merits, but requires phase control of each laser on the order of 1/10 of a wavelength.

Passive coherent beam combining has been demonstrated in which the coherence of each emitter is self-organized^{1,8-10}. The individual elements in a self-organized (passive) CBC array, illustrated in Figure 2, are oscillators of varying optical path lengths with the same output coupler. In the self-organized method, the optical spectrum will adjust to minimize the loss in the array. Another way to state it is to say that the individual emitters mutually injection lock each other at a wavelength within the range for every oscillator. This method has had many demonstrations, however, the combining efficiency falls off as the number of elements is increased^{1,11}. The efficiency as a function of number of array elements is shown in Figure 3 including the predicted mean value of addition efficiency shown with filled circles as well as experimental results shown with open squares.

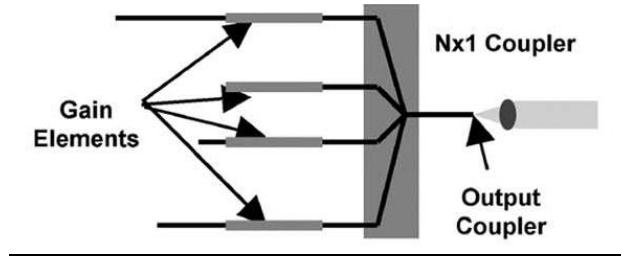


Figure 2: Self Organized Coherent Beam Combining¹

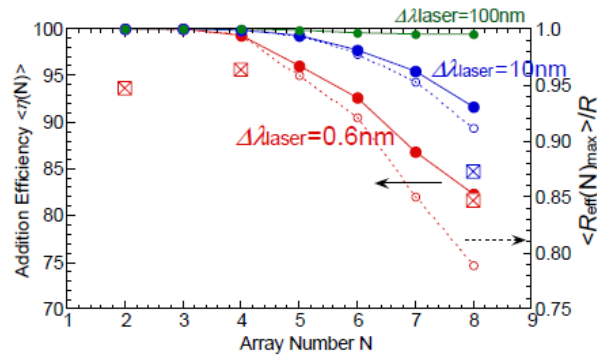


Figure 3: The predicted mean values of the addition efficiency (filled circles) and effective reflectivity (open circles) as functions of the number of array elements. The experimental results are plotted with squares.¹¹

A new approach to passive CBC by multiplexed VBGs has recently been demonstrated, and could provide effective scaling to CBC without the need for ultra-fast electronics to control the phase¹².

Multiple VBGs can be recorded in PTR glass, either at the same wavelength for CBC or at different wavelengths for SBC¹³. In this case the VBGs are recorded for the same wavelength

but at different grating vector angles and with different Bragg angles in the same volume of PTR glass. If all these gratings have a common Bragg angle (degenerated Bragg angle) they form a 1xN splitter/combiner depicted in Figure 4 for the 1x2 case. For such a multiplexed VBG, a beam can be split into N beams, or N properly phased coherent beams of the same wavelength can be combined into one.

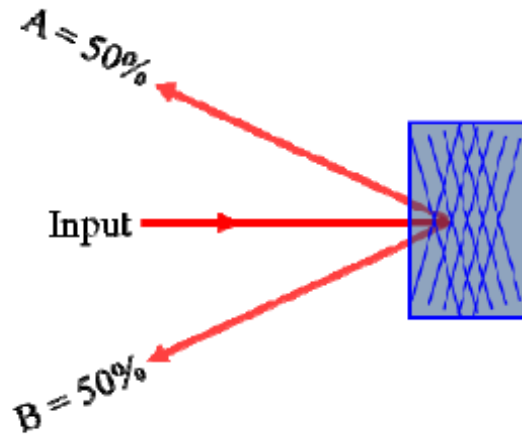


Figure 4: Multiplexed Volume Bragg Grating as 1x2 splitter/combiner ¹²

With this approach, illustrated in Figure 5, mutual feedback between individual gain elements is provided by the VBG that is placed inside the common cavity. The output coupler may be chosen to be the common mirror for all the beams for single aperture output, or the back side mirror for each element to produce an array of passively locked beams.

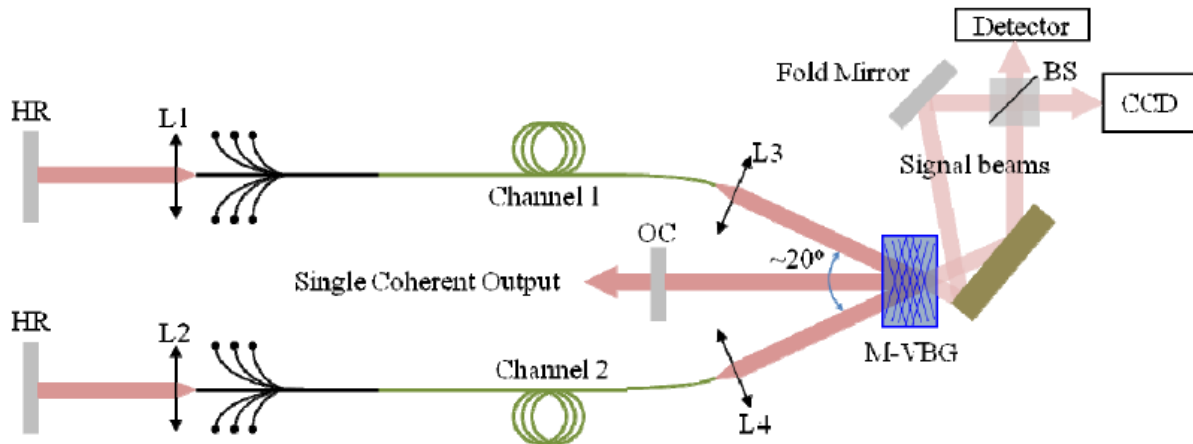


Figure 5: Passive Coherent Beam Combining by Multiplexed Volume Bragg Gratings ¹²

A passive, coherent approach would remove the need for ultra-fast electronics to control the phase of the individual beams. Furthermore, whatever radiance that may be achieved using high power lasers along with CBC, can be increased many times by spectral beam combining of the already coherently combined beams ¹³. In this scheme, the two approaches, coherent and incoherent beam combining, become complementary.

1.2 Survey of Spectral Beam Combining

Spectral beam combining was first proposed in 1970 as a solution for higher bandwidth communications systems ¹⁴. Spectral beam combining systems are essentially the multiplexing part of a wavelength-division-multiplexing (WDM) system. Initially it was proposed that the RF bandwidth of any transmitter or receiver would be limited and therefore multiplexing by

polarization or wavelength would increase the capacity and decrease the technical demand of any transmission system.

Many different approaches were demonstrated, including many free-space and integrated devices¹⁵. Four categories can be discerned from the early demonstrations: angularly dispersive devices^{1, 2, 16 - 47}, wavelength selective filters^{13, 48 - 65}, hybrid devices, and planar waveguide devices⁶⁶. Cross-talk and fiber insertion loss were the major drivers of early development. In high power systems, the goal is to produce a high radiance, free space beam. So fiber insertion loss is not a major concern. Cross-talk however is still a major factor in the development of high power SBC systems. Planar waveguide devices, although compact, and elegant solutions are not an option for high power operation due to their relatively high beam intensity inside the waveguide and the fact that any waveguide device will experience similar thermal and nonlinear limitations that limit the peak power of the individual emitters. Bulk, angularly dispersive devices, such as traditional diffraction gratings, as well as frequency selective filters, such as volume Bragg gratings (VBGs), are excellent options for high power operation. They can be placed inside a multi-laser cavity or be used as combiners outside the cavities of discrete lasers. The majority of recent work in high power SBC has been done with one of these two devices.

1.2.1 Spectral Beam Combining by Angularly Dispersive Elements

1.2.1.1 Introduction to SBC by Angularly Dispersive Elements

Initial attempts at SBC through angular dispersion used prisms, but research moved toward blazed gratings due to their higher dispersion capabilities¹⁵. Traditional diffraction

gratings are a mature technology, historically used for spectroscopy at low powers and wavelength selection inside a laser cavity, but have also been used for SBC and recently at high powers^{17,39}. SBC systems can be designed with intra-cavity, or an extra-cavity combiner. A diffraction grating used in either system can be a transmitting grating or a reflecting grating.

Most SBC systems based on diffraction gratings use an intra-cavity combiner because this serves the dual purpose of combining the beams while supplying wavelength selected feedback to the laser gain medium. In the extra-cavity arrangement, each emitter must have very precise wavelength selection as well as angular and translational alignment. Figure 6 shows transmitting and reflecting configurations for an intra-cavity SBC system.

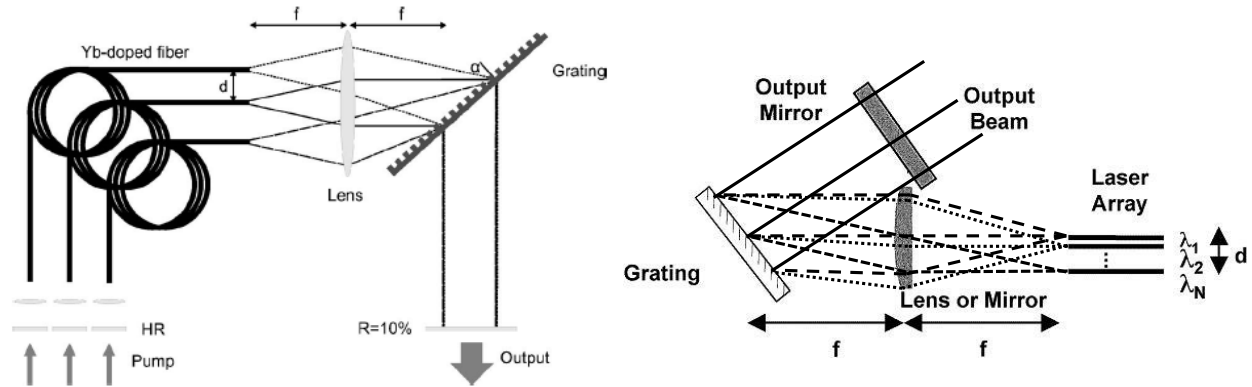


Figure 6: SBC by a transmitting³⁴ (left) or reflecting¹ (right) surface diffraction grating

Whether in the transmission or reflection configuration, parallel beams from individual emitters are focused onto the diffraction grating, which is at the focal distance from the lens. An output coupler is placed normal to the beam path that would provide feedback to the emitters over the desired bandwidth of the system. Each laser will only receive feedback for a specific portion of its gain bandwidth, and will lase at that wavelength. This technique was initially demonstrated with combining of semiconductor lasers¹⁷, but was later used to combine fiber lasers¹⁸, the emitter of choice for recent research due to the high brightness achievable from an individual fiber laser².

Transmitting diffraction gratings have been discarded as an option due to increased thermal distortion of a high power beam passing through the grating substrate². Reflecting diffraction gratings have had moderate success in both high number of combined beams and, in separate experiments, high power beam combining. High beam quality, $M^2 < 1.35$, for combining of 100 emitters has been reported²⁷. This represents a significant increase in radiance of about 66 times the individual emitter radiance. Up to 200 emitters have been successfully combined, but not with near diffraction limited beam quality²⁵. The highest power reported to date for this method was accomplished with four 500 W beams combined to produce a total output power of 2 kW, with $M^2_x = 2.0$ and $M^2_y = 1.8$, and spectral separation between beams of 5 nm³⁹. Unfortunately, the radiance of the combined beam is near that of the initial 500 W input beams.

1.2.1.2 Various Cavity Configurations for SBC by Angularly Dispersive Elements

Many cavity configurations have been demonstrated, but the most common approach is the Littrow configuration. Technically, the Littrow condition for a diffraction grating, illustrated in Figure 7, refers to the condition met when the first diffracting order is angularly overlapped with the incoming beam, and can only be satisfied for a single wavelength at a single angle. This configuration has been used extensively to tune lasers to a desired wavelength⁶⁷⁻⁷¹.

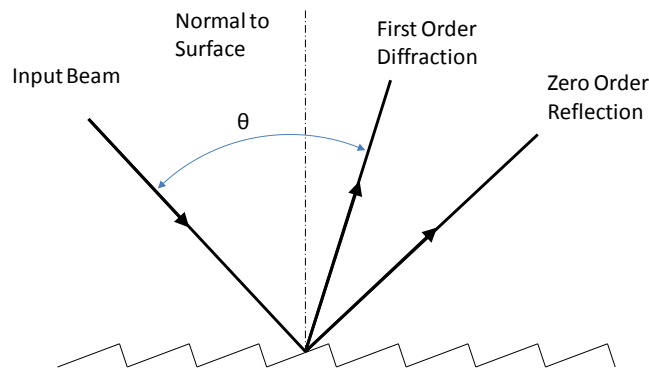


Figure 7: Diffraction grating. Littrow condition occurs for $\theta = 0$ (the 1st diffracted order overlaps with the incident beam)

In the case of wavelength tuning of a single emitter, the beam exiting the gain medium is collimated and the grating is placed in the beam such that the Littrow condition is satisfied for the desired wavelength. If the grating has high diffraction efficiency, the output coupler in this case must be placed on the opposite side of the gain medium⁶⁹. If the grating has low diffraction

efficiency, it can be used as an output coupler and the reflected zero order beam serves as the output beam⁷⁰. These two wavelength tuning arrangements are illustrated in Figure 8.

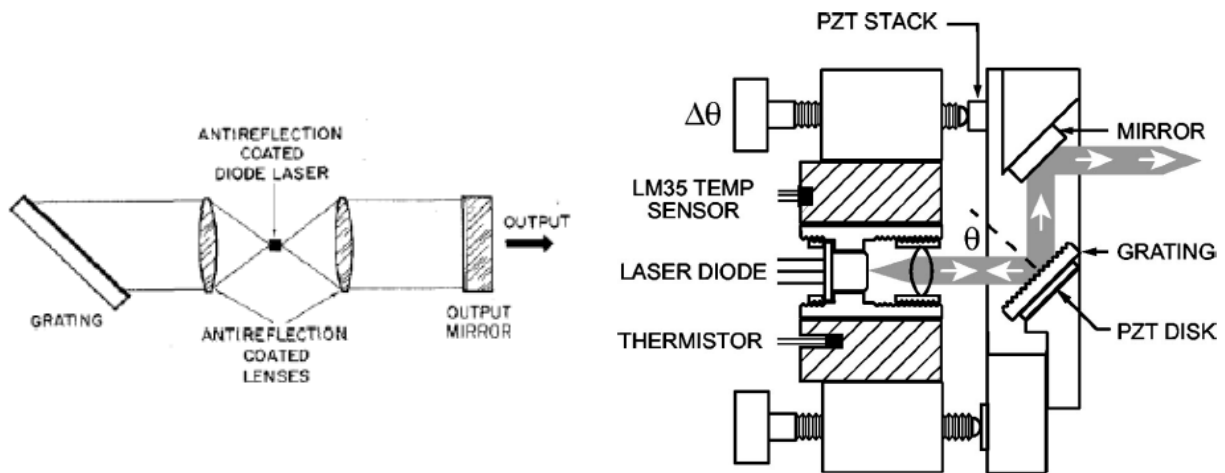


Figure 8: Laser wavelength tuning by gratings used in the Littrow condition for high⁶⁹ (left) and low⁷⁰ (right) diffraction efficiency configurations

A slight adjustment to either case can turn this tuning mechanism into an SBC system. The reflecting configuration in Figure 6 shows a third case in which a diffraction grating period is designed such that the grating only has zero and first diffraction orders. If multiple beams from different gain mediums are collimated, and parallel, but slightly offset in one axis, and a lens is placed in the common beam path, each beam would be sent at different angles to the focus of the lens. If a grating is then placed at the focal spot of the lens, and an output coupler is placed in the zero order beam path, each gain medium would be forced into lasing at a slightly

different wavelength such that the angle it makes with the grating will diffract into the zero order beam. The beams are also forced into parallel output by the fact that the output coupler is flat and normal to the beam path. This method has been used to show high beam quality of combining of 100 emitters²⁷. It is typically used with semiconductor laser arrays, because the arrays can be packed very densely on a single substrate, and combining these arrays of even moderate power of a few watts can increase the brightness considerably.

Another popular method has been preferred by fiber laser SBC systems and is often called the Littrow configuration due to its similar layout and concept to the Littrow configuration used in wavelength tuning of single emitters. Figure 9 shows a variation of this configuration. The only difference being that there is no common output coupler in Figure 9 where the Littrow configuration uses one for common feedback. In this configuration, a Littrow wavelength is selected such that it is in between the wavelengths of the lasers to be combined, and an output coupler is placed normal to the beam that would satisfy the Littrow condition. In this case, individual collimated beams are directed toward the grating at different angles and diffracted toward the output coupler at some wavelength that is adjacent to the Littrow wavelength. This configuration is easiest to understand in reverse. A beam comprised of three wavelengths that are nearby the Littrow wavelength and propagating from the output coupler to the grating will diffract from the grating at three different angles near normal incidence. If these angles are set, then the individual emitters will self-organize or be manually tuned into the proper wavelengths for their respective angles. The output mirror and the diffraction grating are in the common

cavity for each emitter. The highest power examples of fiber laser SBC by surface diffraction grating to date have been using a variation of this configuration^{33,38,39,42}. Figure 9 shows the most common high power configuration which only differs from the Littrow configuration in that there is no common output coupler. The wavelengths and angles of each beam are manually tuned to achieve beam combining rather than being self-organizing.

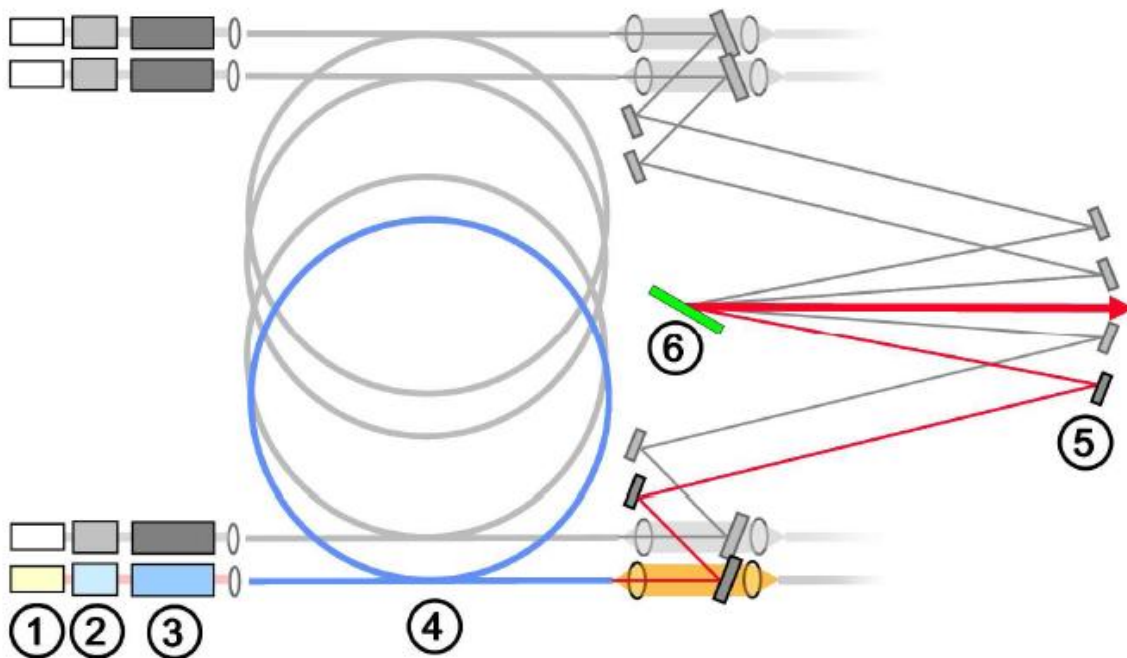


Figure 9: SBC by diffraction grating in “Littrow configuration”. A single channel is highlighted and consists of a seed source (1), a first (2) and second pre-amplifier (3), the main amplifier (4), the folding mirrors (5) and the grating (6).³⁹

As will be discussed later, dispersion is introduced to the individual beams by the grating and can degrade beam quality. An alternate configuration, dual grating SBC³⁶, has been suggested to mitigate the problems associated with the angular divergence of the gratings. In this configuration, shown in Figure 10, individually collimated beams are incident on a grating but translated on the axis of diffraction. The wavelength of each laser is such that the diffracted beams from the first grating are spatially overlapped on a second identical grating. Any dispersion introduced into the beam by the first grating is eliminated by the second grating after which each beam is collinear. Using this method, two low power beams with spectral bandwidth near 0.15 nm were combined. After the first grating each beam had very poor beam quality, $M^2 = 1.9$, while after the second grating the combined beam was diffraction limited, $M^2 = 1.1$. The tradeoff for such a system is increased beam size in the diffraction plane due to angular dispersion between the two gratings and increased system size.

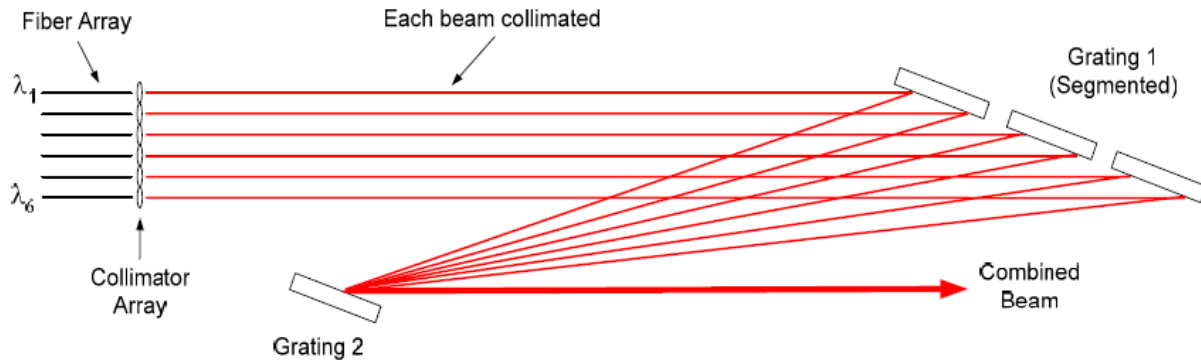


Figure 10: SBC by dual diffraction gratings for beam quality improvement and relaxing of fiber laser bandwidth requirements³⁶

1.2.1.3 Limitations of SBC by Angularly Dispersive Elements

Traditional diffraction gratings are polarization dependent angularly dispersive elements, and are used for their angular dispersion. This same function, however, also contributes to beam quality degradation by introducing additional unwanted dispersion to a beam within a SBC system. This effect is worsened by increasing laser bandwidth as well as increasing dispersion of the grating. Total bandwidth of an SBC system that uses diffraction gratings is limited in part by the dispersion of the grating. This limit is increased with increasing grating dispersion. Grating dispersion should therefore be decreased to improve beam quality but increased to expand the bandwidth of the system. Another factor that has had some attention recently is distortion induced by thermal load on the grating². Thermal distortion can cause deformation of the grating that not only directly deforms the beam through thermal lensing but also distorts the grating

parameters such as grating period. All these factors must be considered when designing high radiance SBC systems by diffraction gratings.

Assuming operation near Littrow condition, beam quality is directly affected by grating dispersion and laser bandwidth as described by Equation 2 below², where ω is the diffraction limited waist radius, $d\lambda$ the laser linewidth, λ the wavelength, Λ the grating period, and θ_L the diffraction angle.

$$dM^2 = \frac{\omega\pi}{2\lambda\Lambda \cos \theta_L} d\lambda \quad (2)$$

Increasing beam width, diffraction angle, laser bandwidth, and decreasing grating period all contribute to a deterioration in beam quality. As an example, a beam with a 1 mm beam radius, 0.1 nm linewidth, and 1030 nm central wavelength incident on a grating at a small angle with an 800 nm grating period would increase M^2 by about 0.20. It's clear that narrow linewidth lasers are required to use this method of beam combining. As discussed above, using the dual grating configuration can reduce this effect at the expense of a larger beam size³⁶.

The total bandwidth available for beam combining is not just limited by the gain bandwidth of the laser medium, but also the application. For atmospheric applications, a transparency window of just 50 nm is available in the near-infrared spectral region around 1 μm . Spectral density becomes very important for such applications.

1.2.2 Spectral Beam Combining by Frequency Selective Filters (VBGs)

Spectral beam combining has been demonstrated by using dielectric thin film interference filters, but even the best performing interference filters cannot match the wavelength selectivity of VBGs^{53,61,72}. Reflecting VBGs in photo-thermo-reflective (PTR) glass are periodic refractive index modulations, recorded by holography, and their design and operation is usually based on Kogelnik's coupled wave theory in thick holograms⁷³.

A complete theoretical model for VBGs based on Kogelnik's coupled wave theory has been developed^{50,74}. Figure 11 and Figure 12 show the propagation of optical rays through a VBG, and the possible orders of diffraction inside the grating for each of the four possible configurations respectively. Many important practical equations resulting from the model for both reflecting and transmitting gratings developed and can be used for modeling VBGs for various designs and uses. These equations will be used for SBC system modeling. An alternate formulation of the coupled wave theory for volume Bragg gratings has been published in order to include Fabry-Perot effects, as well as to include the concept of the strength of a VBG⁷⁵. The analysis that follows in subsequent chapters will be based on the formulation put out by Kogelnik⁷³.

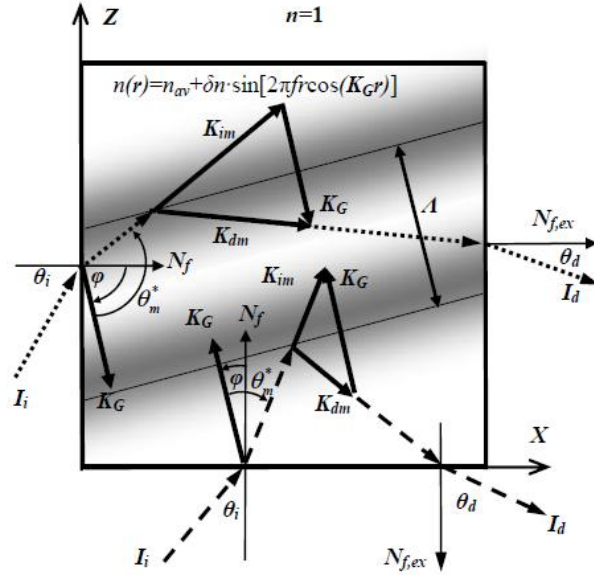


Figure 11: Propagation of optical rays through a volume Bragg grating. \mathbf{N}_f and $\mathbf{N}_{f,ex}$ – normals to the front surface for incident (I_i) and diffracted (I_d) beams; \mathbf{K}_{im} and \mathbf{K}_{dm} – wave vectors of incident and diffracted beams inside the grating medium; \mathbf{K}_G - grating vector; ϕ – grating inclination; θ_i and θ_d – angles of incidence and diffraction; θ_m – Bragg angle; θ_{m^*} – incident Bragg angle.⁵⁰

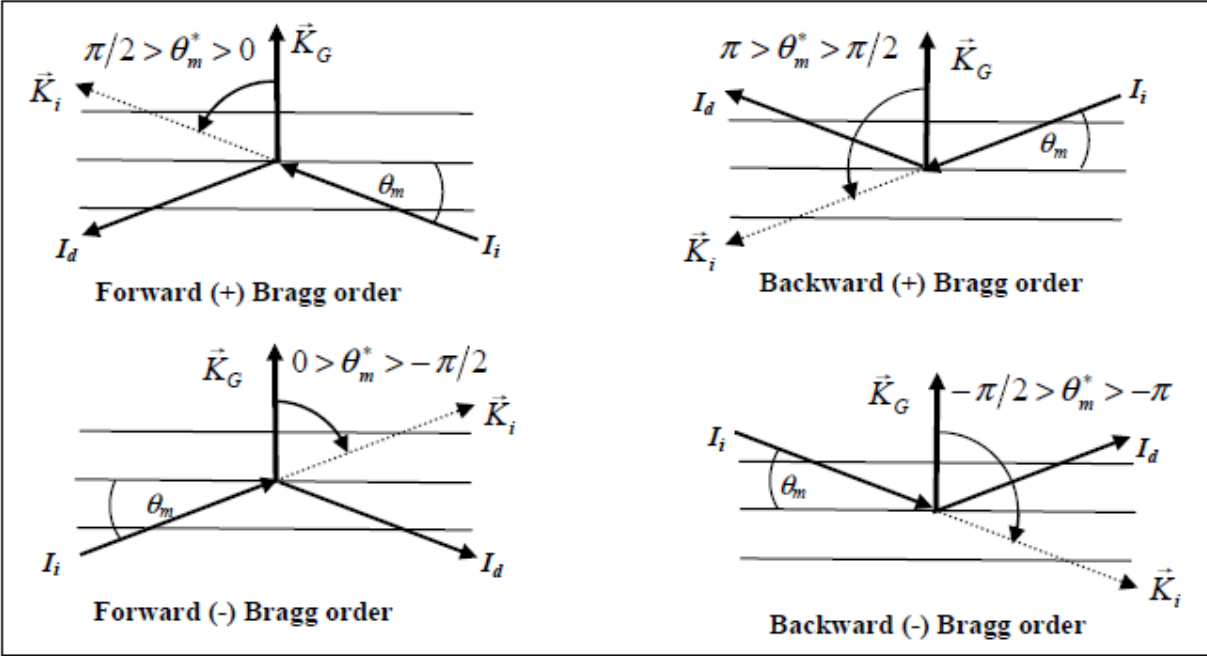


Figure 12: Possible orders of Bragg diffraction inside medium. I_i and I_d —incident and diffracted beams; \vec{K}_i — wave vector of incident beam; \vec{K}_G —grating vector; θ_m — Bragg angle; θ_m^* — incident Bragg angle.⁵⁰

Reflecting Bragg gratings used in a beam combining system fall into the category of frequency selective filters. They are not angularly dispersive, but reflect a beam at some angle for only a narrow range of wavelengths. The properties of these gratings, such as reflection bandwidth, angle, and wavelength, can be tailored to fit the desired system. Diffraction efficiency of VBGs close to 100% has been demonstrated^{53,61,76}. When using VBGs for spectral beam combining, it is important to ensure high diffraction efficiency for the diffracted beam and low diffraction efficiency for the transmitted beams simultaneously. Figure 13 illustrates this concept for the reflecting configuration. The unique, unmatched properties of VBGs allow

achieving this condition at wavelengths with less than 0.25 nm separation, the narrowest spectral separation between beams to date.

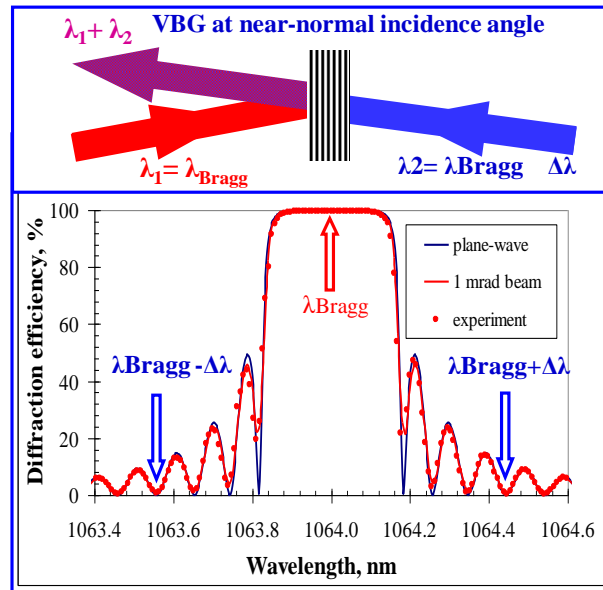


Figure 13: Reflecting volume Bragg grating spectrum for SBC.⁶¹

In the transmitting geometry, two beams of different wavelengths are sent toward the VBG from the same side but at different angles. One beam is sent at such an angle as to be diffracted into a transmitting angle. The second beam is sent at such an angle as to be co-linear with the output angle of the first beam. Because the second beam is not at the Bragg wavelength for that angle, it will completely transmit, and the two beams have combined. This process must be repeated iteratively to combine more beams.

In the reflecting geometry, two beams of different wavelengths are sent toward the VBG from different sides. Just as in the transmitting case, one beam is sent at a resonant wavelength and angle combination such that it is completely reflected. The second beam in this case is sent at the same angle as the output of first beam, and because the wavelength is different, it will transmit with near 100 % efficiency.

For very dense SBC, it is desirable to select a wavelength for the non-diffracting beam such that it falls into one of the minimums of the diffraction efficiency spectrum. This insures high efficiency combining.

SBC by VBGs has commonly been performed outside the laser cavities of individual lasers, and not in an intra-cavity scheme as is common for surface grating efforts. An intra-cavity SBC system with self-organizing wavelength selection has been proposed and demonstrated at low power and is illustrated in Figure 14, but as of yet no high power system has been demonstrated⁵⁶.

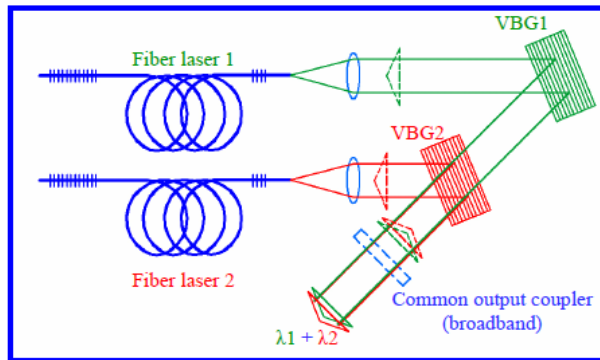


Figure 14: Self organized spectral beam combining by volume Bragg gratings in a common cavity⁵⁶

The first high power demonstration of SBC with transmitting VBGs in PTR glass consisted of two channel combining of 200 W with a wavelength separation of 11 nm, and efficiency of 75 %⁴⁸. Results have improved drastically. Reflecting VBGs have been favored over transmitting VBGs due to the small dispersion that occurs in the transmitting configuration. The best published result for this method is the combining of five 150 W beams with a spectral separation of 0.5 nm between beams, and a total power of 750 W⁵⁶. The architecture for five beam SBC by reflecting VBGs is illustrated in Figure 15. To measure the effect of thermal distortions on the final VBG in the SBC system, a test VBG was placed in the final 750 W beam, and high quality test beam was overlapped with the high power beam and diffracted from the VBG. The beam quality of the test beam, $M^2 = 1.16$, showed no significant distortions.

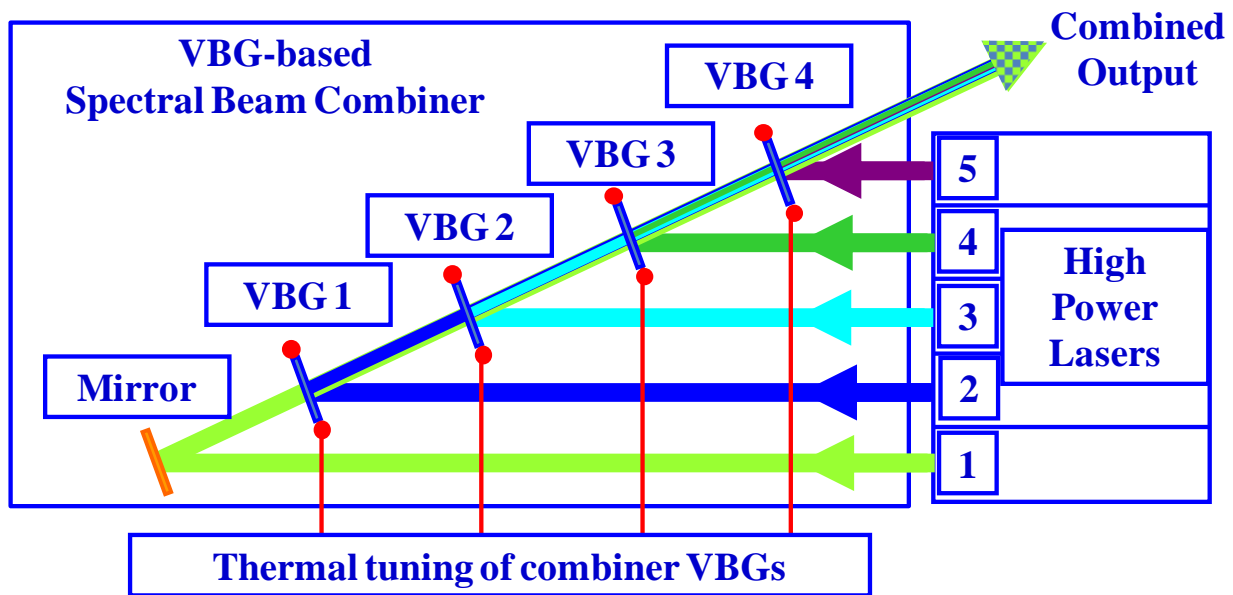


Figure 15: Architecture for five channel SBC by reflecting VBGs

A monolithic SBC apparatus has been proposed and demonstrated that combines five beams in the first stage and four beams in subsequent stages⁶⁰. It would allow modular scaling of SBC by VBGs for as many beams as required. Figure 16 and Figure 17 illustrate these modules. The module can contain a single piece of PTR glass with a multiplexed VBG such that each beam reflects from the VBG at the same output angle, or it can hold a stack of individual VBGs that accomplish the same task. In the demonstration, a stack of VBGs was used, and all four beams were combined with greater than 90 % efficiency.

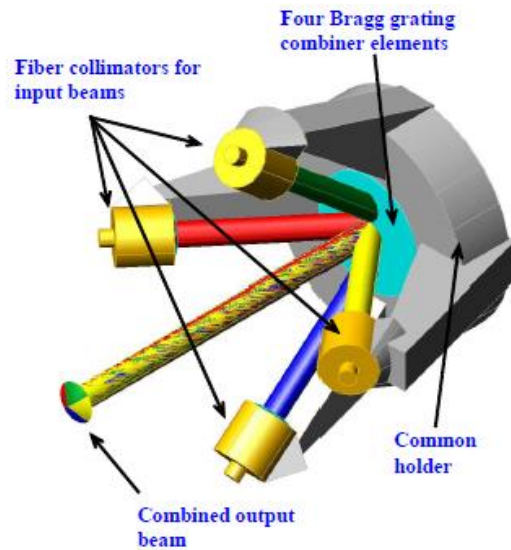


Figure 16: Monolithic SBC module⁶⁰

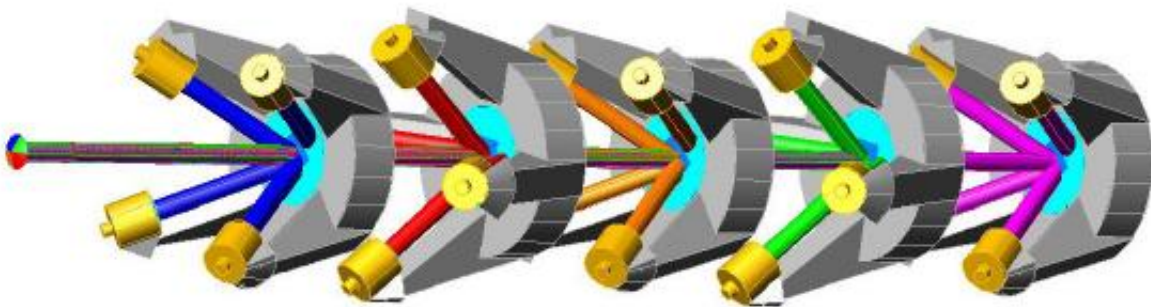


Figure 17: SBC system with stack of five monolithic beam combiners⁶⁰

New major tools and methods, such as SBC system modeling, thermal tuning of VBGs, and beam waist matching, have recently been developed that have led to the most recent high power results⁶⁴, and are presented in this work. New ideas and methods are being considered

and developed, such as SBC by multiplexed VBGs and beam quality improvement with the use of super Gaussian beams. Recent results demonstrating the viability of these new directions are briefly discussed.

2 RADIANCE (BRIGHTNESS) AND THE BEAM COMBINING FACTOR (BCF)

2.1 Radiance (Brightness) Defined

Radiance is defined as the power divided by the product of the solid angle in the far field and the unit area in the beam waist. The radiance for a radially symmetric Gaussian beam is given by Equation 3 below¹.

$$B = \frac{P}{\pi w^2 \pi \theta^2} = \frac{P}{\pi w^2 \pi \theta_{ideal}^2 (M^2)^2} = \frac{P}{\pi w^2 \pi \left(\frac{\lambda}{\pi w}\right)^2 (M^2)^2}$$
$$B = \frac{P}{\lambda^2 (M^2)^2} \quad (3)$$

The M^2 beam quality factor is defined as the measured beam far field divergence divided by the far field divergence of an ideal Gaussian beam with an equivalent beam waist size and is described by Equation 4.

$$M^2 = \frac{\theta}{\lambda/(w*\pi)} = \frac{\theta_{beam}}{\theta_{ideal Gaussian}} \quad (4)$$

It is worth noting that while the radiance is proportional to the beam power, it is inversely proportional to the square of the M^2 beam quality factor. Therefore, for the purposes of obtaining high radiance output beams, it is more important to maintain high beam quality through the combining system than it is to obtain high efficiency if a tradeoff can be made.

Another important consideration when characterizing a high radiance laser system is to consider the spectral radiance which is defined as the radiance per unit wavelength, $B/\Delta\lambda$. If a

beam is intended to propagate through the atmosphere, there are two 50 nm transparency windows in the near IR in which a beam could propagate without being absorbed. Spectral brightness then becomes the figure of merit for a system designed for this purpose.

With Equations 3 and 4, the entire laser system can be characterized in a meaningful way. The goal, however, of both coherent and spectral beam combining systems is to increase the radiance, and the result of different laser systems can be compared by comparing the output radiance.

2.2 Beam Combining Factor (BCF)

If only the beam combining portion of the laser system is to be characterized, the radiance alone cannot accomplish this due to the fact that this also includes characterization of the input beams to the beam combining system.

A metric is needed which considers only the quality of beam combining. Proposed here is the beam combining factor (BCF) which is defined as the radiance of the combined beam divided by the sum of the radiance of the input beams.

$$BCF = \frac{B_{combined}}{\sum B_{unit}} = \frac{(P/M^2)_{combined}}{\sum (P/M^2)_{unit}} \quad (5)$$

By characterizing a beam combining system by the BCF, a beam combining system could be considered to be of high quality, even if low quality inputs beams were used. The BCF ranges from 0-1, where a BCF of 1 is perfect beam combining. If the power of each beam is added into

the final beam without any loss and without any degradation of the beam quality factor, M^2 , then the BCF will be 1. A further simplification can be made to the BCF equation if the input beams are assumed to be equal in power and beam quality. In this case, the BCF depends only on the system efficiency, η , and the ratio between the input beam M^2 factor, and the resulting combined beam M^2 factor.

$$BCF = \frac{(P/M^2)_{Combined}}{\Sigma(P/M^2)_{unit}} = \eta \frac{(M^2)_{Combined}}{(M^2)_{unit}} \quad (6)$$

3 MODELING VBGs FOR HIGH DENSITY SBC

With the necessity of increasingly narrow spectral selectivity, it is important to model VBGs and the effects of non-ideal beams on performance in order to optimize the design of a SBC system. When using VBGs for spectral beam combining, it is important to ensure high diffraction efficiency for the diffracted beam and low diffraction efficiency for the transmitted beams simultaneously. The unique, unmatched properties of VBGs allow achieving this condition at wavelengths with less than 0.25 nm separation. Series 1 in Figure 18 shows the ideal diffraction efficiency spectrum for a VBG. Series 2 through 4 show the result of various non-ideal effects on the diffraction efficiency discussed in more detail below. The far right side of the plot shows the Bragg wavelength at which a beam would be diffracted, while the first minimum in series 1, located at -0.18 nm, shows the location of a possible wavelength at which a beam could be transmitted to combine with the diffracted beam. Without including non-ideal effects in the model, any optimization would produce unrealistic results. A VBG model that includes the three major non-ideal effects, as well as an optimization method for individual VBGs and SBC systems are presented and discussed.

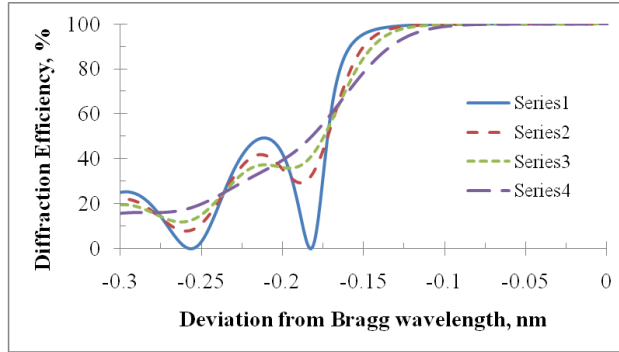


Figure 18: Modeling of VBG diffraction efficiency versus detuning from Bragg wavelength.

First, Kogelnik’s previously developed coupled wave theory for thick holograms is described, including an important adaptation that is necessary for use of the theory in normal incidence cases. Next, a previously unpublished method of simultaneously including the effect of both laser spectral bandwidth and angular divergence on the previously developed coupled wave theory for reflecting VBGs is presented.

3.1 Coupled Wave Theory for Thick Holograms

Kogelnik’s coupled wave theory for thick holograms gives an ideal starting point for a model of reflecting VBGs. Equation 7 below gives the diffraction efficiency as a function of the detuning parameter, ζ , for a reflecting VBG, where n_{av} is the average refractive index in the medium, t is the thickness of the VBG, θ_m is the incident Bragg angle inside the glass, λ_0 is the Bragg wavelength, and δn is the refractive index modulation amplitude.

$$\eta(\zeta) = \frac{\sinh^2(\sqrt{\phi^2 - \zeta^2})}{\cosh^2 \sqrt{\phi^2 - \zeta^2} - \frac{\zeta^2}{\phi^2}} \quad (7)$$

where,

$$\Phi = \frac{2\pi n_{av} t \delta n}{\lambda_0^2 f} \quad (8)$$

and,

$$f = 2n_{av} \frac{\cos(\theta_m)}{\lambda_0} \quad (9)$$

The detuning parameter, ζ , has an angularly dependent and a spectrally dependent component and is given by Equations 10 through 13 below, where Λ is the period of the grating, $\theta = \theta_m + d\theta$, and ϕ is the angle between the grating normal and the glass surface normal.

$$\zeta = -\frac{\vartheta t}{2c_s} \quad (10)$$

$$c_s = \cos \theta_m - \frac{K\lambda_0}{2\pi n_{av}} \cos \phi = \cos \theta_m - \frac{\lambda_0}{n_{av}\Lambda} \cos \phi \quad (11)$$

$$\vartheta = K \cos(\phi - \theta) - \frac{K^2}{4\pi n} \lambda \quad (12)$$

$$K = \frac{2\pi}{\Lambda} = 2\pi f \quad (13)$$

In the following analysis, the grating normal is considered to be perpendicular to the glass surface. Therefore, $\phi = 0$.

A first-order Taylor series expansion of Equation 12 in both dimensions produces the well-known result given by Kogelnik:

The first order Taylor series is given in Equation 14.

$$f(\theta) = f(\theta_m) + \frac{f'(\theta_m)}{1!} (d\theta) \quad (14)$$

Some algebraic manipulation of Equation 12 makes a Taylor series expansion more convenient:

$$\begin{aligned} \vartheta &= K \cos(\theta) - \frac{K^2}{4\pi n} \lambda \\ &= 4\pi n_{av} \frac{(\cos \theta_m)^2}{\lambda_0} \left(\frac{\cos \theta}{\cos \theta_m} - \frac{\lambda}{\lambda_0} \right) \\ &\approx 4\pi n_{av} \frac{(\cos \theta_m)^2}{\lambda_0} \left(\frac{\cos \theta_m + \Delta \cos(\theta)}{\cos \theta_m} - \frac{\lambda_0 + \Delta \lambda}{\lambda_0} \right) \\ &= 4\pi n_{av} \frac{(\cos \theta_m)^2}{\lambda_0} \left(1 + \frac{\Delta \cos(\theta)}{\cos \theta_m} - 1 - \frac{\Delta \lambda}{\lambda_0} \right) \\ &= \vartheta = 4\pi n_{av} \frac{(\cos \theta_m)^2}{\lambda_0} \left(\frac{\Delta \cos(\theta)}{\cos \theta_m} - \frac{\Delta \lambda}{\lambda_0} \right) \end{aligned} \quad (15)$$

A first order Taylor series expansion of $\cos(\theta)$, gives,

$$\cos(\theta) \approx f(\theta) = \cos \theta_m + \Delta \cos(\theta) = \cos \theta_m - (d\theta) \sin \theta_m \quad (16)$$

Therefore, $\Delta \cos(\theta) = -(d\theta)\sin \theta_m$, which gives the commonly used Kogelnik result below.

$$\vartheta = -(d\theta)K \sin \theta_m - (\Delta\lambda) \frac{K^2}{4\pi n_{av}} \quad (17)$$

In this case, the detuning parameter, ζ , becomes:

$$\zeta(d\theta, \Delta\lambda) = \left(\frac{-2\pi n_{av} t \cos \theta_m}{\lambda_0} \right) \left(-d\theta \frac{\sin \theta_m}{\cos \theta_m} - \frac{\Delta\lambda}{\lambda_0} \right) \quad (18)$$

The above result for the detuning parameter is the extent of Kogelnik's developed theory for an ideal VBG. However, if consideration of angular detuning is needed, then this approximation will only work for cases in which $\theta_m \neq 0$. For this reason, it is necessary to include the second order term in the Taylor series expansion for the angular detuning portion. The following is a small adaptation to the above detuning parameter which makes it possible to consider cases in which $\theta_m = 0$. The second order Taylor series is given below.

$$f(\theta) = f(\theta_m) + \frac{f'(\theta_m)}{1!} (\Delta\theta) + \frac{f''(\theta_m)}{2!} (\Delta\theta)^2 \quad (19)$$

In this case, $\Delta \cos \theta = -(d\theta) \sin \theta_m - \frac{1}{2} (d\theta)^2 \cos \theta_m$. This results in a slight modification given in Equation 20 to the commonly used Kogelnik result.

$$\vartheta = -(d\theta)K \sin \theta_m - (d\theta)^2 \frac{K \cos \theta_m}{2} - \frac{\Delta\lambda K^2}{4\pi n_{av}} \quad (20)$$

The resulting detuning parameter that will be considered throughout the rest of this paper is given in Equation 21.

$$\zeta(d\theta, \Delta\lambda) = \left(\frac{2\pi n_{av} t \cos \theta_m}{\lambda_0} \right) \left(d\theta \frac{\sin \theta_m}{\cos \theta_m} + \frac{d\theta^2}{2} + \frac{\Delta\lambda}{\lambda_0} \right) \quad (21)$$

Using Equations 7 and 21, the diffraction efficiency as a function of both angular and spectral detuning can be considered in both normal incidence, $\theta_m = 0$, and off axis, $\theta_m \neq 0$, cases. This form of the detuning parameter allows each dimension to be considered independently. As a result, the effect that non-ideal beam properties, such as divergence and spectral bandwidth, have on VBG performance can be more conveniently considered.

3.2 Modeling Beam Divergence and Spectral Bandwidth Effects in VBGs

3.2.1 Introduction to the Effect of Non-Ideal Beams on VBG performance

There are three main effects that reduce the peak diffraction efficiency at the Bragg wavelength and raise the diffraction efficiency for the transmitted beams: laser beam divergence, spectral bandwidth, and inhomogeneity of the grating parameters across the aperture of the VBG.

Figure 18 shows the influence of these three effects on the diffraction efficiency. The VBG modeled here has a thickness of 3.66 mm and a refractive index modulation of 420 ppm. Series 1 represents the monochromatic plane-wave diffraction by an ideal VBG. Series 2 is for a Gaussian beam with 2 mrad divergence. Series 3 includes 2 mrad divergence and 50 pm laser spectral bandwidth. Series 4 includes 2 mrad divergence, 50 pm bandwidth and 50 pm of

resonant wavelength shift across the aperture. Understanding and minimizing these effects is important to designing an efficient system.

Previously, the effect of laser divergence or bandwidth have been included in the VBG model separately⁷⁴. Accounting for these effects simultaneously as a function of either wavelength or angle in reflecting VBGs has not been previously presented.

3.2.2 Formal Approach to Including Non-Ideal Beam Effects in the VBG Model

To include these effects in the VBG diffraction efficiency profile, the ideal plane wave diffraction efficiency spectrum is first calculated using Equations 7 and 21 that results from Kogelnik's theory of coupled waves described in the previous section^[3].

Finite divergence and finite spectral content must be taken into account for spectral beam combining optimization. To accomplish this, the profile of the input beam in angle space is convolved with the diffraction efficiency followed by a similar convolution in spectral space. Let Equation 22 represent the input beam in spectral space with a Gaussian spectral profile, and Equation 23 represent the input beam in angle space with a gaussian divergence profile, where w is the spectral width, θ_0 is incident beam angle, and b is the divergence (FW $e^{-2}M$).

$$G_{\lambda}(\Delta\lambda, w) = e^{-2\left(\frac{\Delta\lambda - \lambda_0}{w}\right)^2} \quad (22)$$

$$G_{\theta}(d\theta, b) = e^{-2\left(\frac{d\theta - \theta_0}{b}\right)^2} \quad (23)$$

In previous approaches, a single convolution in either wavelength space, or angle space was suggested, however, to include both effects, a double convolution must be carried out in series. It does not matter which is performed first. For convenience of computation, which will become clear later, the convolution in angle space will be done first. Let $\eta_{d\theta}(d\theta, \Delta\lambda)$ in Equation 24 represent the diffraction efficiency as a function of both wavelength and angle after convolution with $G_\theta(\Delta\theta, b)$.

$$\eta_{d\theta}(d\theta, \Delta\lambda) = \frac{(G_\theta[d\theta, b] * \eta[d\theta, \Delta\lambda])(d\theta)}{\int G_\theta[d\theta, b] d(d\theta)} \quad (24)$$

The effects of a beam with a finite spectral bandwidth may be included simultaneously by convolving $\eta_{d\theta}(\Delta\theta, \Delta\lambda)$ with $G_\lambda(\lambda, w)$.

$$\eta_{d\theta, \Delta\lambda}(d\theta, \Delta\lambda) = \frac{(G_\lambda[\Delta\lambda, w] * \eta_{d\theta}[d\theta, \Delta\lambda])(\Delta\lambda)}{\int G_\lambda[\Delta\lambda, w] d(\Delta\lambda)} \quad (25)$$

Finally, the variations in VBG Bragg wavelength across the beam aperture can be included in the model by the same mathematical method. If the shift in Bragg wavelength as a function of a lateral coordinate is assumed to be nearly linear, and the beam is Gaussian, Equation 25 can be used again to account for this shift, where w is now the spectral shift in Bragg wavelength across the beam aperture.

A third convolution is necessary to incorporate all three effects into the model simultaneously. Equation 26 results from performing a second wavelength convolution on Equation 25.

$$\eta_{\Delta\lambda_b, d\theta, \Delta\lambda}(d\theta, \Delta\lambda) = \frac{(G_{\lambda_b}[\Delta\lambda, w] * \eta_{d\theta, \Delta\lambda}[d\theta, \Delta\lambda])(\Delta\lambda)}{\int G_{\lambda_b}[\Delta\lambda, w] d\Delta\lambda} \quad (26)$$

Equation 26 gives the VBG diffraction efficiency as a function of wavelength detuning and Bragg angle, including the effects from beam divergence, beam spectral bandwidth, and a Bragg wavelength shift across the beam aperture.

3.2.3 Computational Implementation of Simultaneous Angle and Wavelength Convolutions

The model is designed to be used for optimization. In this case, it is important to maintain a high speed implementation. The numerical convolution process in angle space described here is illustrated in Figure 19. The diffraction efficiency spectrum is calculated for each Bragg angle, θ_m , within a range of interest, producing a two dimensional diffraction efficiency array. In this array, the horizontal index, N, represents wavelength change while the vertical index, M, represents angle change. To include the effects of a divergent beam, a one-dimensional array representing the angular distribution of the beam is generated from Equation 23 and is multiplied row by row in angle space to the diffraction efficiency array. This is not a matrix dot or cross product, but an element by element multiplication of a one-dimensional array to each row of a two-dimensional array. Then the area under each row is divided by the area under the curve generated by Equation 23. This operation is illustrated in Figure 19. The resulting one dimensional array is the diffraction efficiency as a function of wavelength including the effects of a finite beam divergence. Equation 27 gives the formal

equivalent of the described operation. This operation effectively convolves Equations 23 and 7 in angle space, and can be performed in milliseconds by an up to date personal computer.

$$\eta_{d\theta}(\Delta\lambda) = \frac{\int_{-\infty}^{\infty} G_{\theta}[\tau,b]\eta[\tau+d\theta,\Delta\lambda]d\tau}{\int_{-\infty}^{\infty} G_{\theta}[\tau,b]d\tau} \quad (27)$$

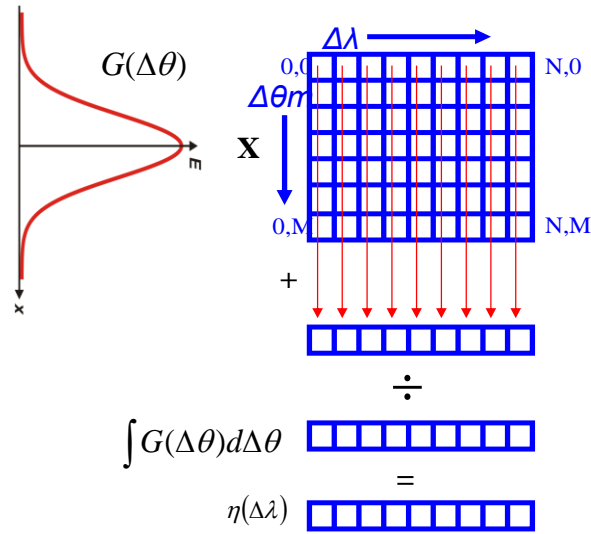


Figure 19: Numerical convolution in angle space

The following convolutions in wavelength space are performed in a similar manor, but because the diffraction efficiency spectrum is in a numerical form rather than analytical after the previous convolution, it becomes convenient to use the Gaussian beam spectrum as the shifting function. Instead of multiplying a single gaussian shape to many Bragg wavelength shifted VBG diffraction efficiency spectra, the resulting VBG spectra from the angle-space convolution is

multiplied to an array of wavelength shifted Gaussian beams in wavelength space. The formal notation for this operation is shown in Equation 28, and the process is illustrated in Figure 20. Note that convolution is commutative. So it does not matter which of the two functions involved in the convolution is used with a shifting variable in the integral.

$$\eta_{d\theta,\Delta\lambda}(\Delta\lambda) = \frac{\int_{-\infty}^{\infty} G_{\lambda}[\tau+\Delta\lambda,w]\eta_{d\theta}[\tau]d\tau}{\int_{-\infty}^{\infty} G_{\lambda}[\tau,w]d\tau} \quad (28)$$

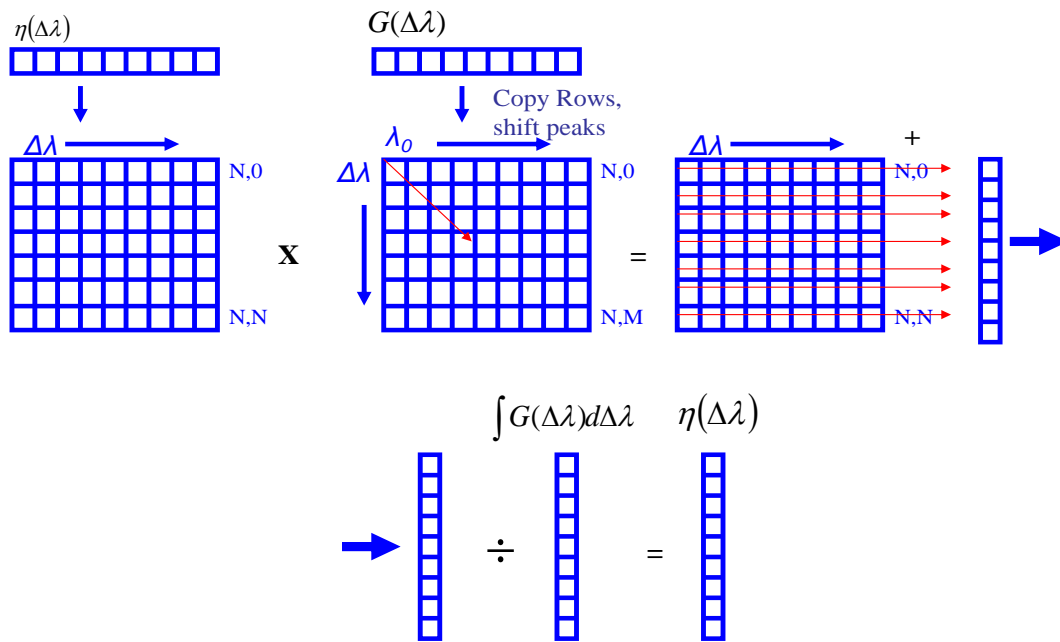


Figure 20: Numerical convolution in wavelength space

3.2.4 Experimental Verification of Beam Divergence, and Bandwidth Effects on VBG Performance

A VBG with refractive index modulation, $\delta n = 102.81$ ppm, and thickness, $t = 3.99$ mm, and a Bragg period at normal incidence of 531.81 nm, is used to diffract a tunable laser at normal incidence with diffraction limited divergence, and a spectral bandwidth of 0.114 nm (full width $\frac{1}{e^2}$). Figure 21 shows both the theoretical modeling and experimental measurements which show very close matching, indicating that the effect of beam spectral divergence on diffraction efficiency is accurately modeled.

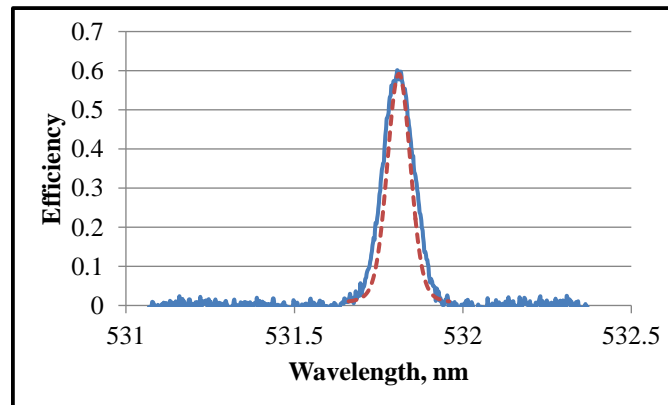


Figure 21: Comparison Theory(dash) v.s. Experiment (solid); VBG refractive index modulation = 102.5 ppm, Bragg Period = 531.81 nm, thickness = 3.99 mm; Laser spectral bandwidth = 0.144 nm, divergence = diffraction limited.

To further confirm the method, a VBG with $\delta n = 415$ ppm, and thickness, $t = 3.50$ mm, and a Bragg period at normal incidence of 1066.57 nm, is used to diffract a tunable

laser at an angle of 7.9° (half angle) with 23 mrad divergence (full angle), and a single frequency spectral bandwidth. The focus of the beam was placed at the surface of the VBG so as to rule out any effect of VBG inhomogeneity. Figure 22 shows the comparison of theory and measurements which match very closely and confirms that the effect of beam divergence on VBG performance is accurately modeled.

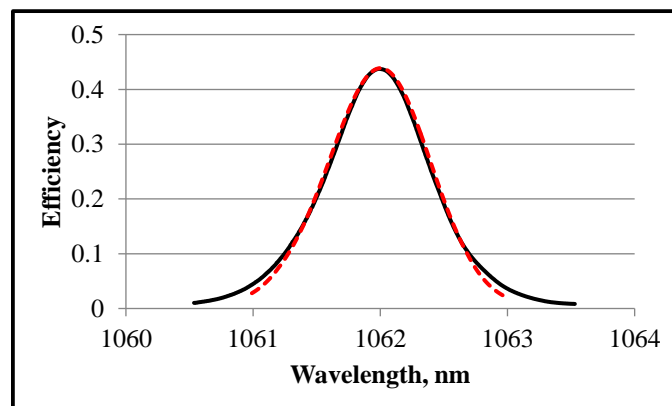


Figure 22: Comparison Theory(dash) v.s. Experiment (solid); VBG refractive index modulation = 415 ppm, thickness = 3.5 mm, Bragg Period = 1066.57 nm; Laser spectral bandwidth < 20 pm, divergence = 23 mrad (full width)

4 OPTIMIZATION OF VBG PARAMETERS FOR SBC

4.1 Single Stage Optimization

A method for optimizing a spectral beam combining system with an arbitrary number of channels has been developed. In the previous section, modeling the diffraction efficiency spectrum for a single grating was discussed. The results of this modeling are used to optimize a single VBG for SBC. For a given number of laser beams, each with finite divergence and bandwidth, with a given spectral separation, starting wavelength, and a possible range of grating thickness and refractive index modulation, a grating configuration is found to achieve maximum efficiency. The finite divergence and bandwidth of the beams are major parameters that drive the optimization, and must be accounted for in the manner described in the previous section.

In a SBC system, illustrated in Figure 15, there are as many VBGs as beams minus one. In this case, optimization must be performed for each VBG. The first VBG in the SBC system will only interact with two beams, the diffracted beam at the VBG resonant wavelength, and the transmitted beam at some specified distance from the resonant wavelength. The next VBG in the system will interact with three beams, the diffracted beam at the VBG resonant wavelength, and the two beams from the first VBG which will both transmit through the second VBG. This continues until the desired number of beams is combined.

Initially, the case of one VBG with one reflecting beam and one transmitting beam will be considered. The same method can then be adapted to multiple beams, and, through an iterative process, to multiple VBGs in a SBC system with an arbitrary number of beams.

As was illustrated in the previous section, and can be seen in Figure 23, diffraction performance can be affected by beams with some finite spectral bandwidth or divergence. The goal of an optimization is to maximize total efficiency with respect to both the transmitting and reflecting beams. Given a certain beam divergence, the diffraction efficiency at the Bragg wavelength will be reduced from the ideal case, which will reduce the efficiency of the reflected beam. The transmission efficiency of beams to be transmitted through the minima in the diffraction efficiency spectrum will also be reduced. An increase in either the VBG thickness or the refractive index modulation will have the effect of further increasing the peak diffraction efficiency at the Bragg wavelength and decreasing the transmission efficiency at the minima in the spectrum.

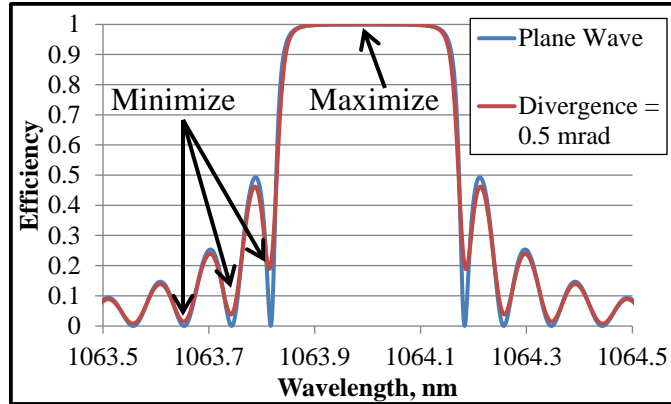


Figure 23: Diffraction efficiency spectrum for plane wave, and 0.5 mrad (half angle) divergent beam

The optimal thickness and refractive index modulation for a VBG intended to diffract one beam, and transmit one beam at some specific spectral separation must be found such that a balance between increasing diffraction efficiency at the Bragg wavelength and increasing transmission efficiency at a desired minimum is achieved.

To optimize such a VBG, a spectral separation between beams is chosen, 0.25 nm for example, as well as a divergence for the beams, 0.5 mrad (half angle) for example, assumed to be the same for both. Given such parameters, a set of diffraction efficiency spectra, $\eta_{d\theta}(\Delta\lambda, t, \delta n, b)$ from Equation 24, including the effects of divergent beams, should be calculated for a range of thickness and refractive index modulations, where $\Delta\lambda$ is the detuning parameter in wavelength, t is the VBG thickness, δn is the refractive index modulation, and b is the full angle divergence of the input beams. For each calculated diffraction efficiency spectrum,

the beam combining efficiency should be determined by Equation 29 below, where λ_B is the Bragg wavelength, and λ_T is the transmission wavelength such that $\lambda_B - \lambda_T = \Delta\lambda_s$ which is the spectral separation between beams.

$$\eta_{BC}(t, \delta n) = \frac{1}{P_B + P_{T_1}} \left[P_B (\eta_{d\theta}(\lambda_B, t, \delta n, b)) + P_{T_1} (1 - \eta_{d\theta}(\lambda_{T_1}, t, \delta n, b)) \right] \quad (29)$$

This approach can be easily expanded to an arbitrary number of transmitting beams and one reflecting beam interacting with one VBG by the more general equation for beam combining efficiency given by Equation 30.

$$\eta_{BC}(t, \delta n) = \frac{1}{P_{in}} \left[P_B (\eta_{d\theta}(\lambda_B, t, \delta n, b)) + P_{T_1} (1 - \eta_{d\theta}(\lambda_{T_1}, t, \delta n, b)) + \dots + P_{T_N} (1 - \eta_{d\theta}(\lambda_{T_N}, t, \delta n, b)) \right] \quad (30)$$

Equation 31 gives a more concise notation, where N is the number of transmitting beams interacting with the VBG being optimized, P_B is the power of the reflecting beam at the Bragg wavelength, P_{T_N} is the power of the Nth transmitting beam, and P_{in} is the total power incident on the VBG.

$$\eta_{BC}(t, \delta n) = \frac{1}{P_{in}} \sum_{n=1}^N \left[P_B (\eta_{d\theta}(\lambda_B, t, \delta n, b)) + P_{T_n} (1 - \eta_{d\theta}(\lambda_{T_n}, t, \delta n, b)) \right] \quad (31)$$

.Equation 31 can now be used to generate a two dimensional array of beam combining efficiency of a VBG as a function of VBG thickness and refractive index modulation for a specified number of beams, N, at a specified spectral separation, $\Delta\lambda_s$, with a specified beam

divergence, b . An example of the resulting data can be seen in Figure 24. The software interface that was created as a part of this research is shown in Figure 25. A search for the maximum combining efficiency through the resulting data will produce the optimized values for thickness and refractive index modulation.

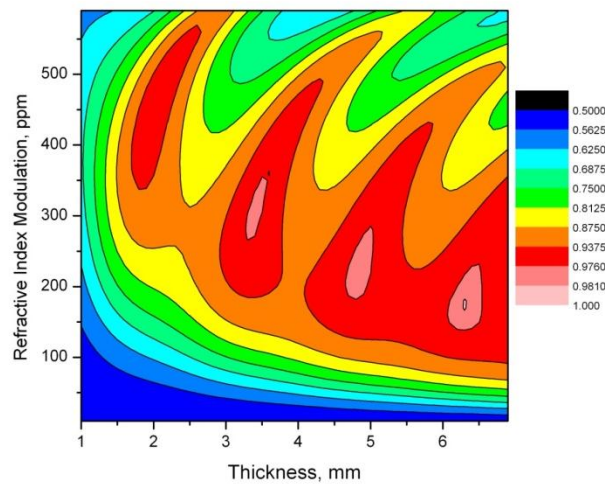


Figure 24: Combining efficiency, single stage SBC, 2 beams, 0.25 nm separation, 0.5 mrad div (half angle)

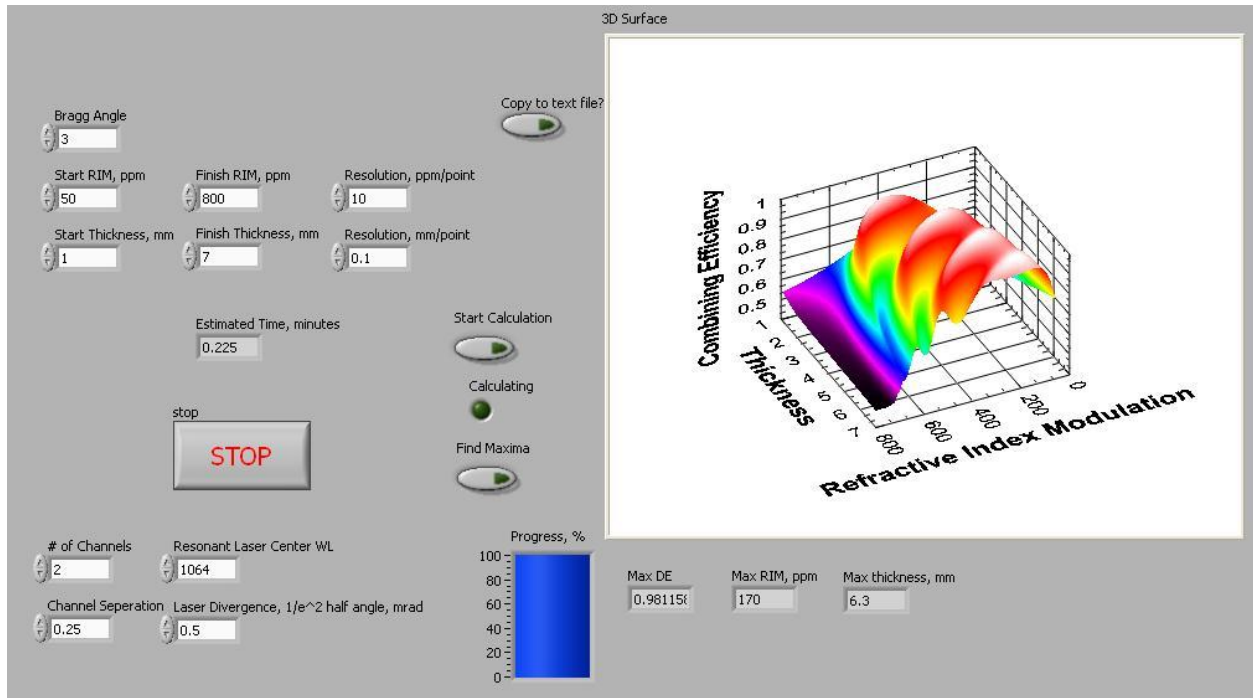


Figure 25: Software interface for VBG optimization

Unfortunately, for each thickness-refractive index modulation combination, equation 31 must be calculated which requires a 1000×1000 diffraction efficiency matrix for sufficiently accurate calculations during the convolution with the Gaussian shape of the beam's divergence. A modest 100 points along the thickness axis and 100 points along the refractive index axis will require 10,000 convolutions for a single stage SBC system. For a standard office computer, this will require hours to calculate. Although this is possible to use, it can be impractical, and as it turns out, unnecessary.

The lasers used for the spectral beam combining experiments that will be discussed in detail in a later chapter are single frequency lasers, and in general high power fiber lasers are available with a spectral bandwidth of less than 20 pm. If such lasers are used, then the bandwidth of the lasers has a negligible effect on the VBG performance, and can be neglected. However, even diffraction limited beam divergence on sub-10 mm diameter beams can have an effect on the VBG diffraction efficiency spectrum, and must be taken into account.

So, for the sake of speed, and the demonstration of the concept, it will be assumed that the input lasers are single frequency, and therefore the diffraction efficiency calculation and convolution in angle space can be made for only the specific wavelengths at which the lasers operate. This reduces the required matrix size from 1000×1000 to 1000×2 for a 2 beam SBC system. Furthermore, it is not necessary to perform the convolution in angle space for a broad angle range. If, the calculated angle range is reduced to three times the full width of the beam divergence, the calculation matrix can be reduced to 250×2 for a 2 beam, 1 VBG optimization, and more generally $250 \times N$ for an N beam, 1 VBG system. This reduces the calculation to less than 1 ms for each data point generated by equation 31, and allows for optimization within 1 minute for a single VBG optimization.

Another important factor in optimization is to include losses associated with increasing thickness and refractive index modulation. Both scattering and absorption have been observed in PTR glass, but scattering losses are orders of magnitude higher than absorption, and for the

purposes of determining efficiency and optimizing the VBG parameters, only scattering losses will be considered. In the linear regime, $\Delta n < 600 \times 10^{-6}$, the scattering loss coefficient in PTR glass is given by Equation 32 below, where $\Delta n = 2 * \delta n$ and $L(750nm)$ is the scattering loss coefficient at 750 nm wavelength.

$$L(750nm) = \frac{\Delta n}{10000} \quad (32)$$

The loss coefficient at another wavelength is given by the following expression.

$$L(\lambda)_{cm^{-1}} = L(750nm) \left(\frac{750nm}{\lambda} \right)^4 cm^{-1} \quad (33)$$

The loss percentage is calculated by the following equation.

$$L(t) = (1 - 10^{-L(\lambda)_{cm^{-1}} \times t}) \quad (34)$$

Including the scattering loss of Equation 34 into the combining efficiency calculation of equation 31, yields the following expression for combining efficiency.

$$\eta_{BC}(t, \delta n) = \frac{(1-L(t))}{P_{in}} \sum_{n=1}^N \left[P_B(\eta_{d\theta}(\lambda_B, t, \delta n, b)) + P_{T_n} (1 - \eta_{d\theta}(\lambda_{T_n}, t, \delta n, b)) \right] \quad (35)$$

Some interesting conclusions can be made after some key optimization calculations. This discussion is still focused on examining only a single VBG with a single reflecting beam and multiple transmitting beams with a divergence of 0.5 mrad (half angle), and spectral separation of 0.25 nm between beams.

A two beam example was already shown in Figure 24. The maximum combining efficiency was calculated to be 98.1 % at 6.3 mm thickness and 170×10^{-6} refractive index modulation for a range 0 to 7 mm and 50 to 800×10^{-6} respectively. If, however, the analysis is extended to a maximum thickness of 25 mm, an absolute maximum combining efficiency of 98.3 % can be found with a thickness of 19.9 mm and a refractive index modulation of 60×10^{-6} . An absolute maximum can also be found for higher numbers of transmitting beams. The same analysis performed for a total of five beams results in a maximum of 98.5 % combining efficiency at 16.8 mm thickness and 60×10^{-6} refractive index modulation is found.

The reason that the five beam case results in a higher efficiency at a smaller thickness, is that more of the total power in the system is transmitting through the minima in the VBG spectrum rather than diffracting from the peak at the Bragg wavelength. In this case the optimization is weighted toward slightly weaker VBGs such that the peak in the diffraction efficiency spectrum is slightly lower, and the transmission efficiency of each of the four transmitting beams is slightly higher.

It is clear that if a VBG could be made with thicknesses in the range of 20 mm with high quality, an absolute maximum in combining efficiency could be achieved. However, it is not very beneficial to go to such thicknesses as will become clear with the next set of examples.

Referring back to Figure 24, four peaks in the combining efficiency can be seen as a function of thickness and refractive index modulation, but the peaks appear mostly in the

thickness direction. These peaks in combining efficiency represent a combination of thickness and refractive index modulation such that the transmitting beam that is nearest in wavelength to the Bragg wavelength of the reflecting beam falls into the first, second, third, or fourth minimum of the diffraction efficiency spectrum. The solution with the thinnest grating represents the use of the first minimum, and the solution with the thickest grating represents the use of the fourth minimum. These minima can be seen in the diffraction efficiency spectrum of Figure 23.

If the optimization analysis is limited to a maximum thickness of 3 mm, the first peak in combining efficiency can be found, and results in a maximum of 97.40 % combining efficiency at a thickness of 2.1 mm and refractive index modulation of 470×10^{-6} . As discussed in the previous paragraph, the first peak in combining efficiency corresponds to using a VBG thickness and refractive index modulation such that the transmitting beam that is nearest in wavelength to the Bragg wavelength falls in the first minimum of the diffraction efficiency spectrum. Analysis of the second peak shows a combining efficiency of 97.97 % at a thickness of 3.4 mm and δn of 310×10^{-6} , a gain of 0.57 %. Examining the third peak shows a combining efficiency of 98.06 % at a thickness of 4.8 mm and δn of 220×10^{-6} , a gain of only 0.09 %. The fourth peak shows a combining efficiency of 98.12 % at a thickness of 4.8 mm and Δn of 170×10^{-6} , a gain of only 0.06 %. These examples are specific to beam divergences of 0.5 mrad (half angle), and single frequency lasers with 0.25 nm spectral separation. For beams with higher divergence, or with greater than 25 pm of bandwidth, the differences in combining efficiency for successive peaks

will be exaggerated, the use of thicker gratings utilizing higher order minimums for transmission may be called for.

It is worth pointing out that the next contour down from the highest efficiency contour in Figure 24 is set to be only 0.5 % below the peak in beam combining efficiency. So rather than there being a single solution, VBGs manufactured in the range shown by this contour level will produce reasonably high beam combining efficiency.

In the case of nearly collimated beams, and single frequency lasers, the gain in combining efficiency after the third peak is only 0.06 %. As stated before, the third peak in combining efficiency corresponds to the use of the third minimum in the diffraction efficiency spectrum for the transmitting beam that is nearest to the Bragg wavelength of the reflecting beam. Thicker VBGs are more difficult to manufacture than thin VBGs, and accumulate more laser induced heat during operation. Therefore, thinner VBGs are desirable if a compromise can be reached. Based on the examples discussed in this paragraph, there is a significant performance advantage in using the third minimum, but the advantage diminishes with each successive minimum. It is concluded that optimization should be made to find the thickness and refractive index modulation associated with the third peak in combining efficiency.

4.2 N-Stage Optimization

The optimization analysis up to this point has been with regard to a single stage of an SBC system. Even for cases in which more than two beams were considered, one beam would

be reflecting from one VBG, while the remaining beams were transmitting through the same VBG. A multi-beam, VBG-based, SBC system will have as many VBGs as beams minus one. Optimization is performed iteratively for each successive VBG in the system. The output of each iteration, which is the ratio of the power incident on the optimized VBG to the power that will arrive at the next VBG for each beam, is used as the input for the next iteration. The final result of the optimization is the necessary refractive index modulation and thickness for each VBG in the system to obtain peak combining efficiency. Figure 26 illustrates the iterative optimization.

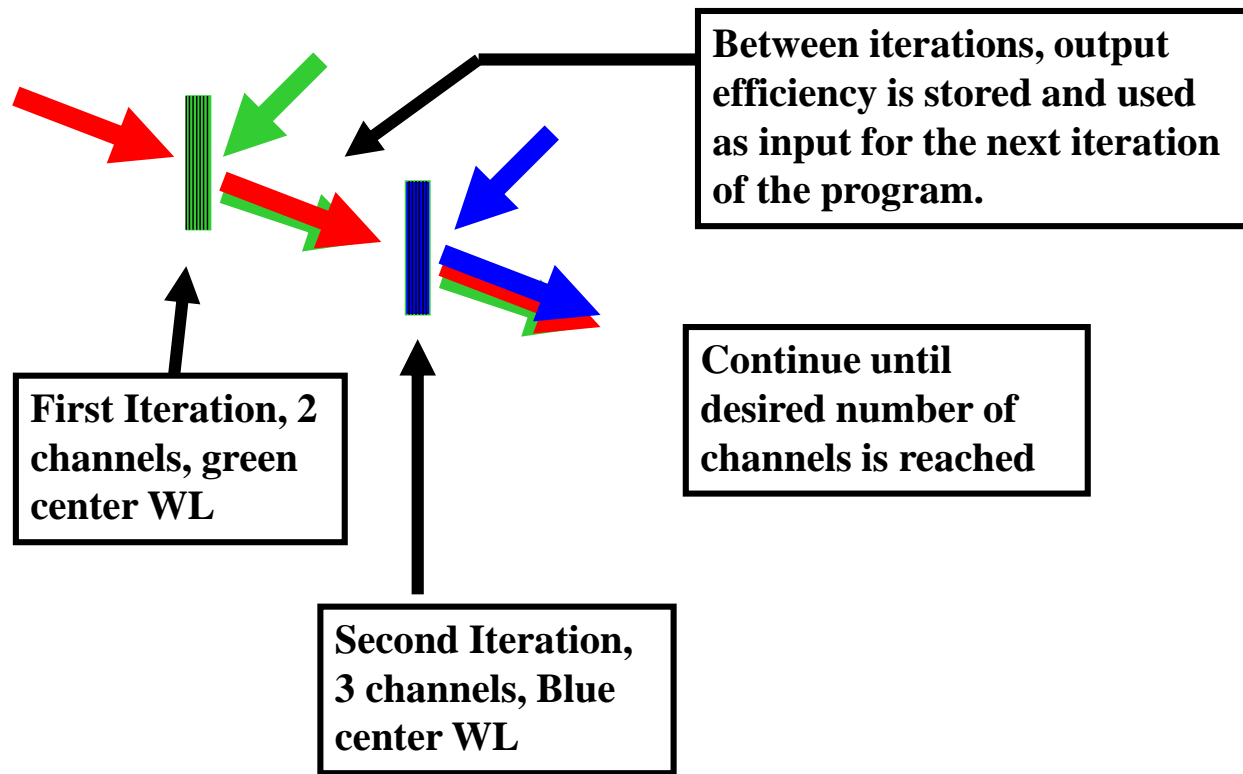


Figure 26: Illustration of iterative SBC system optimization

Figure 27 shows an example of the resulting data from an optimization calculation for a 5-channel combining system with a spectral separation between channels of 0.25 nm around 1064 nm, and beam divergence of 0.5 mrad (half angle).

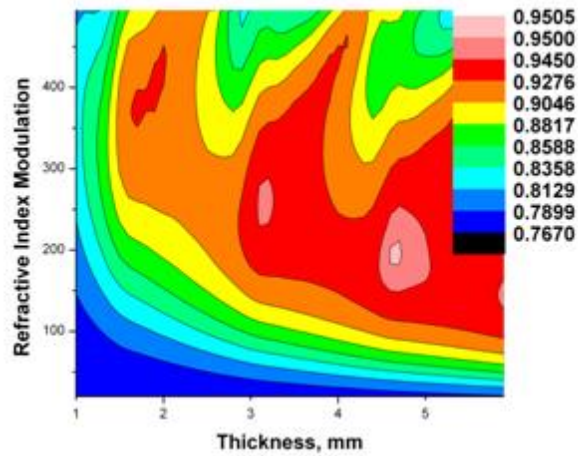


Figure 27: Efficiency of 5-channel SBC as a function of VBG thickness and refractive index modulation

The ideal diffraction efficiency for each of the four VBGs whose parameters were determined by the optimization procedure is shown in Figure 28. This system was designed such that each laser would interact with every VBG whose Bragg wavelength is less than or equal to that of the laser. Every VBG in Figure 28 has less than 1% diffraction efficiency at wavelengths corresponding to the Bragg condition of higher-wavelength VBGs.

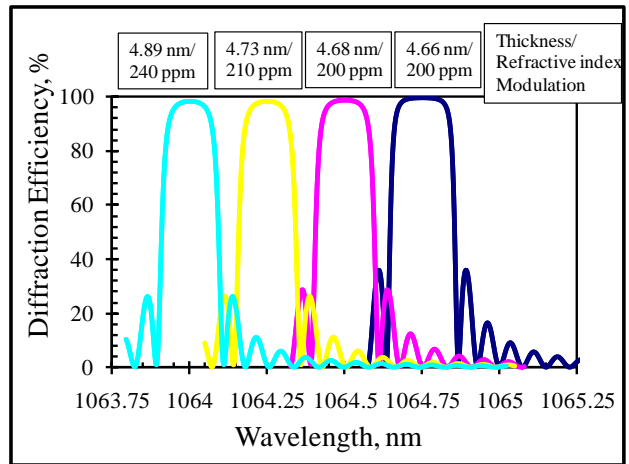


Figure 28: Diffraction efficiency spectra of VBGs for an optimized system

5 MODELING THE BEAM QUALITY OF COMBINED GAUSSIAN BEAMS

Laser induced heating of VBGs can introduce slight expansion of the grating period, lensing, and thermally induced aberrations. The expansion of the grating period can be compensated by thermal tuning which will be discussed in detail in a later chapter. Thermally induced lensing can be compensated by telescopes on the input beams, but to what precision does lensing need to be controlled? Higher order aberrations induced by laser heating can effect the beam quality of each beam separately due to the fact that each VBG experiences a different thermal load, and each beam transmits through a different number of VBGs. A model for calculating beam quality in the form of the M^2 factor is presented in which individual beam waist mismatch due to thermal lensing is considered, as well as the effect of differing beam quality in each beam due to higher order thermally induced aberrations.

5.1 Modeling the Combined M^2 of Ideal Gaussian Beams with Beam Waist Mismatch

Laser induced heating of the VBGs introduces very slight focusing to each beam, and these changes will be unique for each beam. The focal length of the thermally induced lenses will vary depending on incident laser power and the absorption of the glass used. In the cases considered in this dissertation, the focal lengths of the induced lenses have been approximated to be a few meters to tens of meters depending on the particular experiment and which beam is considered. These small differences in beam divergence will not degrade the M^2 of the individual beams, but, if left without compensation, the composite M^2 after combination can be

adversely affected if the beams do not have equivalent divergence at the output of the system⁷⁷. Beams of different divergences can be described in terms of having different effective waist locations and sizes. This effect can be measured when focusing the beams to form a new beam waist in order to measure the beam quality.

To illustrate the effect beam waist mismatch between beams can have on beam quality, two collinear beams with slightly different divergences, but $M^2 = 1$, are modeled and the combined beam quality is calculated. Figure 29 shows the beam $\frac{1}{e^2}$ size as a function of propagation distance from the aperture for two beams with different divergences (half angle), $\theta_1 = 0.1129$ mrad, and $\theta_2 = 0.2129$ mrad, but each with diffraction-limited beam quality, $M^2 = 1$. The aperture size is 3 mm for both beams at $z = 0$.

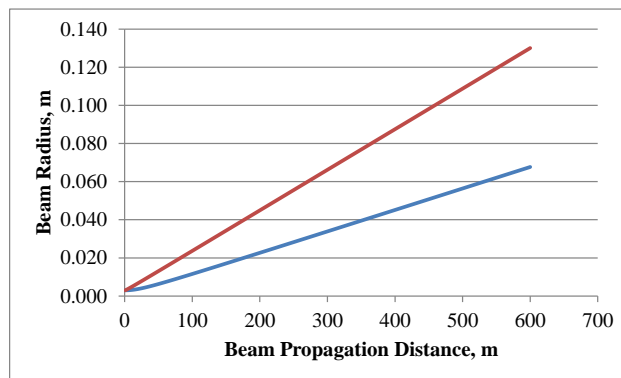


Figure 29: Beam radius v.s. propagation distance for two beams with a divergence difference of 0.100 mrad

In order to determine the combined beam quality factor, M^2 , the intensities of each beam must be summed at two points in the far field. The divergence can then be calculated from the beam size at each point. The beam quality factor can then be determined by dividing this divergence by the divergence of an ideal Gaussian beam with the same aperture size. Figure 30 shows the relative intensity of each beam as a function of beam radius after 10 meters of propagation. Even though the areas under these curves are identical, the peak power of the higher divergence beam has significantly reduced at this point, but the combined beam quality, $M^2 = 1.25$, has not yet been reduced to an unusable level.

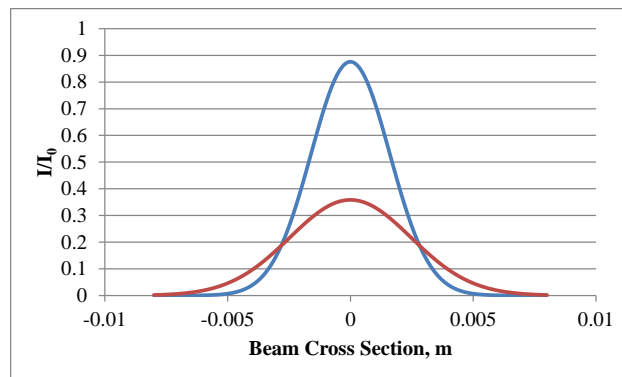


Figure 30: Cross section of two beams with 0.100 mrad divergence difference after 10 m propagation

This value was calculated using the second moment beam radius in the far field at two different points in z and comparing the divergence of the combined beams with the divergence of

an ideal diffraction limited beam. The intensity profile of each beam in the far field is calculated using Equation 36 below, P is the power; z, the propagation distance from the aperture; z_r , the Rayleigh length; $w(z)$, the beam radius at some distance z; and λ , the wavelength.

$$I = \frac{P}{1 + \left(\frac{z}{z_r}\right)^2} e^{-2\left(\frac{r^2}{w^2(z)}\right)} \quad (36)$$

where,

$$z_r = \frac{\pi w_0^2}{\lambda} \quad (37)$$

and,

$$w(z) = w_0 \sqrt{1 + \left(\frac{z}{z_r}\right)^2} \quad (38)$$

After each beam profile is generated in the far field, they are summed incoherently to provide the profile of the combined beam. For a Gaussian beam of any divergence, the divergences calculated by the $\frac{1}{e^2}$ beam width or by calculating based on the second moment, σ^2 , beam width are identical. However, in this case, two Gaussian beams with different divergences are summed and the result is not a Gaussian shape. The second moment method of calculating the beam divergence must be employed.

The beam radius, w , of a given intensity profile can be calculated by finding the variance as described in Equation 39.

$$W_{\text{combined}} = \sqrt{2\sigma^2(z)} = \sqrt{2 * \frac{\int_0^{2\pi} \int_0^{\infty} r^2 I_{\text{combined}}(r,z) r dr dz}{\int_0^{2\pi} \int_0^{\infty} I_{\text{combined}}(r,z) r dr dz}} \quad (39)$$

The same calculation is made for a perfect Gaussian beam at the same points in z. The half angle divergences are calculated for each and are compared to determine the combined beam quality as given in Equation 40.

$$M_{\sigma}^2 = \frac{\phi_{\sigma_{\text{combined}}}}{\phi_{\sigma_{\text{gaussian}}}} = \frac{(\sqrt{2\sigma^2(z_2)} - \sqrt{2\sigma^2(z_1)})_{\text{combined}}}{(\sqrt{2\sigma^2(z_2)} - \sqrt{2\sigma^2(z_1)})_{\text{gaussian}}} \quad (40)$$

Figure 31 shows the relative radiance as a function of the M^2 beam quality factor for different quantities of combined beams. The relative radiance is calculated as the combined beam radiance, determined by use of Equation 1, divided by the radiance of an individual input Beam. Relative radiance is related to the beam combining factor, BCF, by dividing the relative radiance by the number of beams. From the plot, it can be seen that for two beams with an $M^2 = 1.25$, the increase in radiance is about 30 %, and a BCF of 0.64. Ideally the radiance would increase by 100 % for each beam that is combined which can be seen in the plot for $M^2 = 1$. If the divergence difference between the two beams is reduced to 0.050 mrad, the combined beam propagation factor is improved to $M^2 = 1.16$ which gives about a 50 % increase over the single beam radiance, and a BCF of 0.74. To achieve a 90 % increase in radiance by combining two beams, the necessary difference in divergence between the beams that must be maintained is less than 0.010 mrad, which corresponds to $M^2 = 1.03$

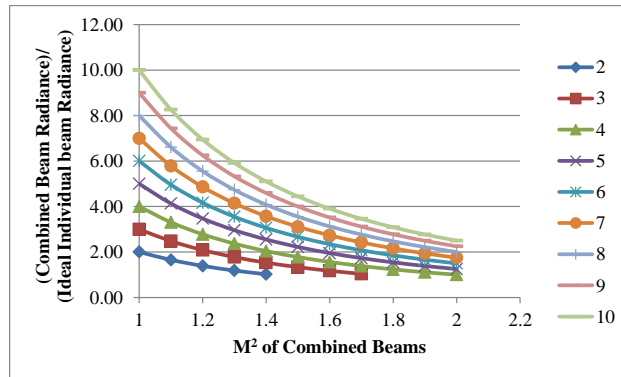


Figure 31: Relative Radiance in a combined beam v.s. M^2 for individual beams.

It is clear that to effectively increase the radiance of spectrally combined beams, the divergence of each beam must be tightly controlled. The results are slightly different for five beams due to the fact that a smaller portion of the power will be located in the lowest or highest divergence case. Figure 32 shows the beam $\frac{1}{e^2}$ size as a function of propagation distance from the aperture for five beams with different divergences, 0.113 mrad, 0.138 mrad, 0.163 mrad, 0.188 mrad, and 0.213 mrad, for a total difference in divergence equal to that of the two beam case, 0.100 mrad. Figure 33 shows the intensity cross-section of the five beams after 10 meters of propagation. The combined beam quality factor for all five beams is calculated to be $M^2 = 1.34$, which gives a BCF of 0.56. Table 1 summarizes the findings for both the two and five beam cases.

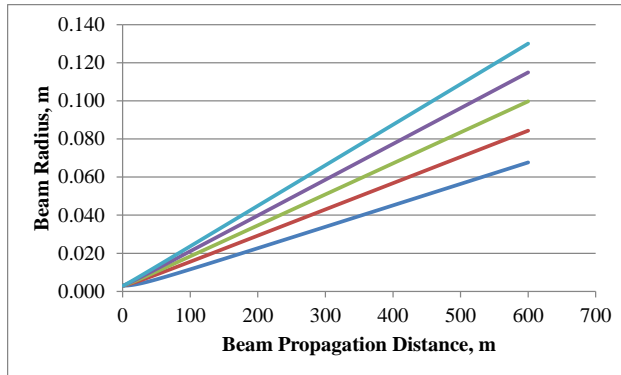


Figure 32: Beam radius v.s. propagation distance for five beams with a total divergence difference of 0.100 mrad

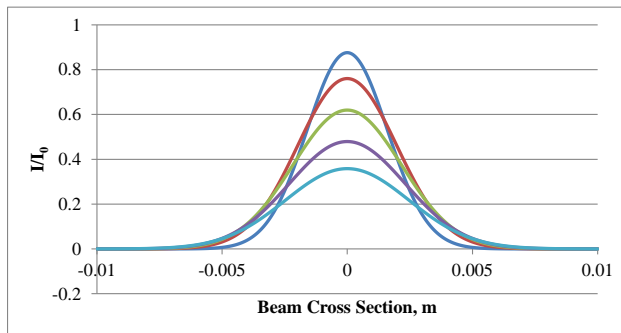


Figure 33: Cross section of five beams with 0.100 mrad total divergence difference after 10 m propagation

Such small differences in divergence are difficult to measure, and the divergence for each case would be different for different size beams. For this reason it is often better to sample the beam, focus it to form a new waist, and measure the focal spot error at the waist. For purely first order spherical aberrations, defocus, each beam will simply have a shifted waist with a different

size. If the beam divergences were perfectly aligned, the waists would occur at the same location and would have the same radius.

The procedure to precisely align the beams should be to match the location of the beam waists in the focal spot after a lens, ideally in the same location as a diffraction-limited test beam. If this is achieved, any measurement of far field divergence will show equal, diffraction-limited divergence for all beams involved, and a combined $M^2 = 1$, assuming that the initial beams are diffraction-limited and no higher order aberrations are added by the beam combining optics. It is concluded that an error in focal spot of up to $\frac{1}{2}$ of a Rayleigh length does not cause significant degradation of the beam quality factor or relative radiance.

5.2 Ideal Alignment of Non-Ideal Beams, $M^2 \neq 1$

In the previous section, tolerances on beam divergence differences for ideal diffraction-limited beams where $M^2 = 1$ for each beam were discussed. In most high power cases the beam quality of each beam will not be ideal, and in the case of VBG-based spectral beam combining, each beam experiences a different set of distortions due to the fact that each beam transmits through a different set of VBGs that are each being heated by different optical power loads. The beam that transmits through all VBGs will have higher distortions than the final beam which only diffracts from a single VBG.

In this case, it is impossible for a beam with $M^2 > 1$ to be adjusted to have diffraction-limited divergence. By definition, the minimum divergence for that beam would be increased by

a factor of its M^2 . $M^2 = \frac{\phi_{beam}}{\phi_{ideal-gaussian}}$. If the far field divergence is measured for each beam, the only way to give the beams equal divergence would be to increase the divergence of the beams with better beam quality which would result in a shifting of the beam waists in the focal spot and the combined beam quality would be reduced. In the case of ideal beams of different divergence, the divergence could be measured directly, and each beam adjusted to be equal; but in the case of non-ideal beams the best case is not when the divergences are equal, but when each beam has the smallest possible divergence.

A clear method to achieve this is to ensure the beam waists in the focus are aligned together. The beam radius at the waist will be a different size for each beam that has a unique beam quality, but the waist locations should be aligned to the location of the ideal Gaussian beam waist. This insures that the divergence for each beam is as close to ideal as possible and the combined beam quality is best in this case.

Table 1: Summary of beam propagation factor, divergence, Rayleigh length, and radiance findings for two and five beam spectral beam combining

2-Beams			
Divergence Difference, mrad	0.100	0.050	0.010
Combined M^2	1.25	1.16	1.03
Focus Error/Rayleigh Length	1.60	1.04	0.43
Relative Radiance	1.28	1.49	1.89
BCF	0.64	0.74	0.94
5-Beams			
Divergence Difference, mrad	0.100	0.050	0.010
Combined M^2	1.34	1.19	1.04
Focus Error/Rayleigh Length	1.60	1.04	0.43
Relative Radiance	2.78	3.53	4.62
BCF	0.56	0.71	0.92

5.3 Experimental Setup for Beam Waist Measurement of Spectrally Combined Beams

As discussed above, VBGs are recorded in PTR glass which has a small but finite absorption. This absorption causes each VBG to heat up and expand. The expansion induced by heating changes the Bragg wavelength and must be tuned by thermal tuning devices that are discussed in detail in the chapter on thermal tuning of VBGs. The thermal tuning devices operate by cooling the edges of the VBG until the center of the VBG returns to the correct temperature and hence thickness to achieve the Bragg condition for the desired wavelength. This process can maintain the efficiency from low to high power operation, but, although the temperature in the center of the VBG is maintained, the temperature gradient across the aperture of the VBG causes the VBGs to behave like thermal lenses with a very long focal length.

Ideally, each laser in the system could be tuned individually while all other lasers are turned off. However, since the lensing and aberrations are caused by heating from all lasers, the alignment must be made while the system is at full power. This introduces a significant complication to the problem of aligning the beam divergences. All five lasers in the beam combining system should be propagating collinearly if properly aligned, and the spectral separation between beams is only 0.25 nm. A demultiplexer must be employed in order to separate each beam for measurement and alignment.

A new approach has been developed in which a thermally tuned VBG with wavelength selectivity of 0.25 nm is used as the spectrally selective filter. Unlike the VBGs in the beam combining portion of the setup, this VBG can be tuned across the entire spectral range of the system, 1 nm, due to its high temperature range, from 5° C to 130° C. The high power combined beam is sampled down to a lower power and sent into the measurement setup. After a beam is selected and reflected from the demultiplexing VBG, it is sent through two alignment mirrors, and a beam sampler before being measured for waist size, divergence, and beam quality factor, M^2 . Figure 34 illustrates the experimental setup. The beam sampler sends a portion of the beam into an integrating sphere where the power and spectrum are analyzed to ensure that the proper beam has been selected.

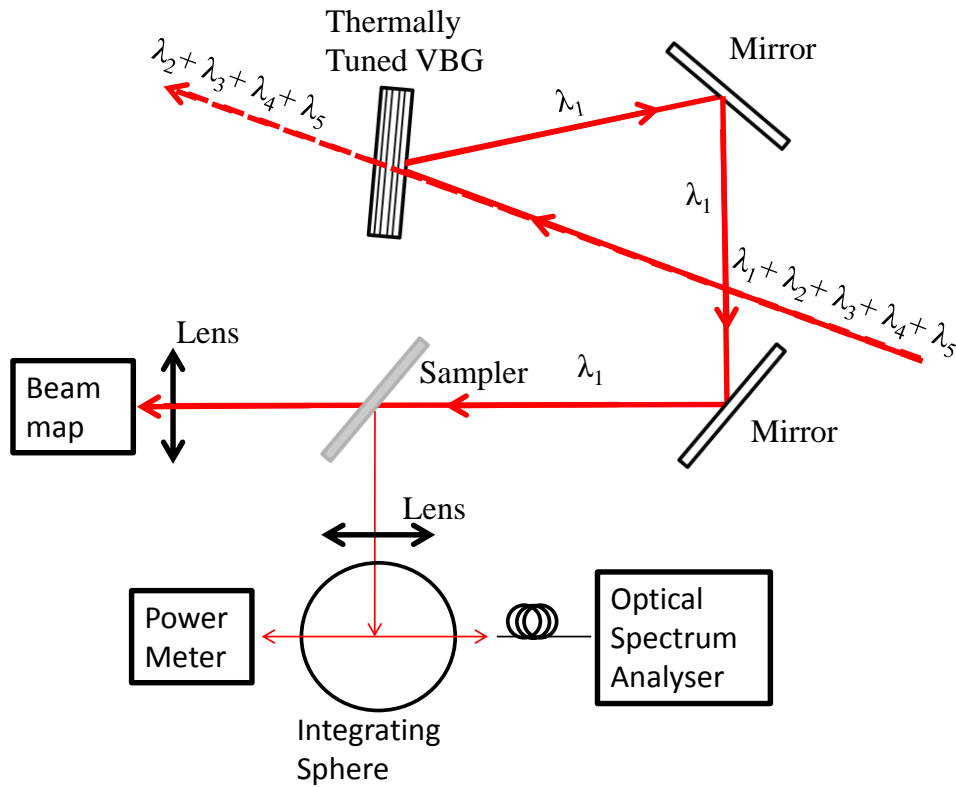


Figure 34: Demultiplexing and beam measurement experimental setup

Before sending the combined beam into the measurement setup, an ideal, low power, diffraction-limited Gaussian beam is sent into the Beam Map to determine the ideal focal spot for a perfect beam, $M^2 = 1$. The divergence of each of the five combined beams in the system can now be selected by the demultiplexing VBG, and adjusted until the focal spots are all in the same locations after the analyzing lens. In this way each beam will achieve the smallest divergence possible and the best combined beam quality can be reached. This technique is used to align the divergence of five 150 W beams with a spectral separation between beams of 0.25 nm.

6 THERMAL TUNING OF VOLUME BRAGG GRATINGS

A thermal tuning technique has been developed for maintaining high efficiency of beam combining throughout the power range of the system. VBGs are recorded in PTR glass which has a small but finite absorption. It means that the glass is heated under high power laser radiation, which causes glass expansion and hence Bragg wavelength shift. Therefore, when the system is aligned to operate with high efficiency at low power it must be re-aligned for high power beams to produce high combining efficiency. Using the new thermal-tuning technique, initial alignment is performed while heating the VBGs with a novel heating apparatus. As laser power is increased, the VBG temperature is lowered, and combining efficiency is maintained without need for mechanical adjustment. The thermal tuning apparatus is shown in Figure 35.

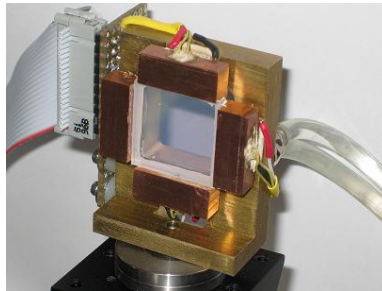


Figure 35: VBG thermal tuning apparatus

An additional advantage to thermal tuning of the VBGs is very precise tuning of the grating period. To effectively combine high power beams with such a narrow spectral

separation, very precise control of the VBG resonant wavelength must be implemented. VBGs with narrow spectral selectivity also have narrow angular selectivity. So tuning the VBGs by angle becomes a challenge and is impractical at high output powers. By changing the temperature of the VBG, the glass expands or contracts, changing the period of the VBG and hence the resonant Bragg wavelength. This thermal method of tuning the resonant wavelength has much greater resolution than angle tuning and, once implemented, can be controlled electronically. A thermal tuning method and novel thermal tuning apparatus is presented in order to achieve precise control of the VBG resonant wavelength and hence combining efficiency of a SBC system without mechanical tuning.

To demonstrate the need for thermal tuning of VBGs for high spectral density SBC, Figure 36 shows the calculated diffraction efficiency spectrum for a VBG with parameters consistent with those used in the SBC system, thickness of 4.78 mm, refractive index modulation of 211 ppm, and approximately 65 pm of Bragg wavelength shift across the beam aperture of 6 mm. The desired transmission wavelength is the third minimum of the VBG's efficiency spectrum and is 0.25 nm from the Bragg wavelength. The beam is assumed to be monochromatic and have diffraction-limited divergence.

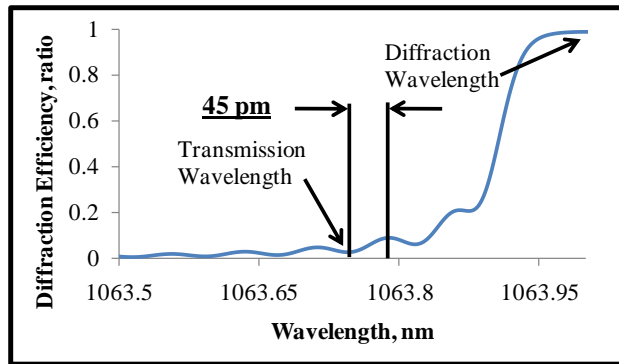


Figure 36: The tail of a diffraction efficiency spectrum illustrating sensitivity of losses for a transmitting beam to offset of wavelength

The wavelengths at which beams are to be transmitted and diffracted are highlighted in Figure 36. It is important to note that in the area of the side lobes, the distance between nearest maxima and minima of reflection efficiency is only 0.045 nm. A wavelength offset of this value would reduce transmittance of the grating by 7 %. The diffracting beam would also experience a reduction in efficiency for a 0.045 nm tuning error, but there would only be a reduction in efficiency of around 2 %. Maintaining very precise control of the Bragg wavelength is important for the diffracting beam but critical for the transmitting beam.

Due to the necessity of high wavelength precision, the tuning apparatus must have high thermal stability. Figure 37 shows the measured temperature in the copper attachments at the edge of the VBG during temperature control. The temperature was set to 70 degrees, but the resulting average temperature was approximately 68.7 °C, and the standard deviation was 1.0 °C. The deviation of the measured average temperature and the set point temperature is not

extremely important as the SBC system is aligned with respect to the actual temperature at the center of the VBG not necessarily the set temperature at the edge. The alignment procedure will be discussed in greater detail. Even though the standard deviation is only 1.0 °C this is the deviation at the copper at the edge of the VBG. Copper has significantly higher thermal conductivity than the glass. This suggests that the temperature variation at the center of the glass will be damped with respect to the measured temperature variation in the copper at the edge. It can be reasonable concluded that the temperature variability in the center of the VBG will be significantly less. Even if considering the 1.0 °C variation in the copper, this only represents a 0.01 nm deviation which is within a reasonable tolerance for the proposed system with 0.25 nm spectral separation.

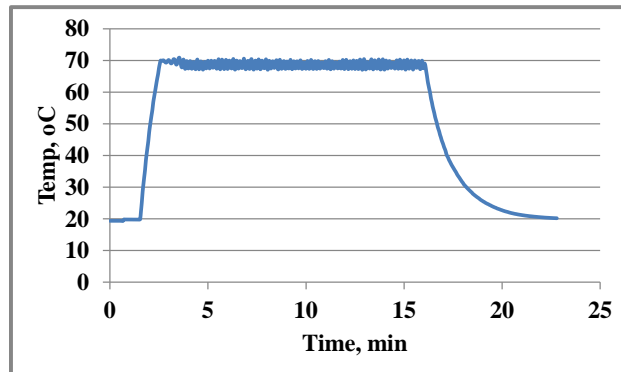


Figure 37: Temperature stability of TEC while controlling a VBG. At the 70 °C set point the average temperature was 68.7 °C, and the standard deviation was 1.0 °C.

In order to probe the VBG behavior while under various heating conditions, a test beam is overlapped on the VBG with the high power beam such that the diffraction efficiency spectrum of the VBG with or without laser induced heating at various edge temperatures can be determined.

The experimental setup is shown in Figure 38. The high power laser produces a 6 mm, 160 W beam, while the low power tunable laser produces a 6 mm, ~10 mW, beam with close to diffraction limit divergence. Heating to the grating may be caused by both the high power laser beam and the external heating apparatus. The diffraction efficiency spectra are measured with the tunable low power laser under various heating conditions.

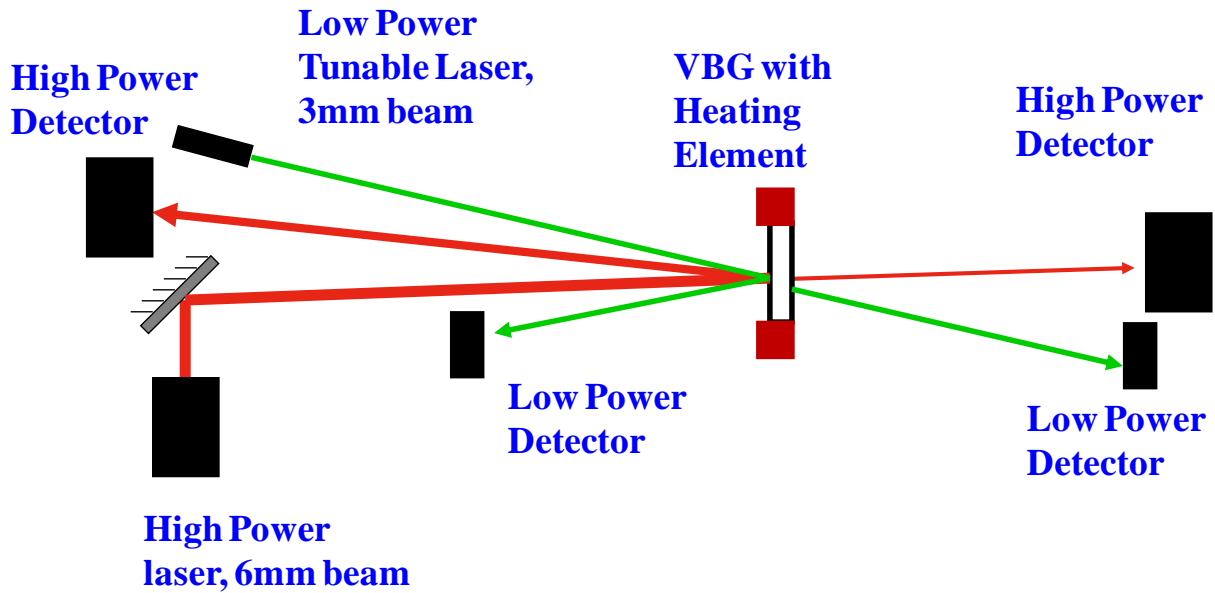


Figure 38: Experimental setup for diffraction efficiency spectra measurement in VBGs exposed to high power laser radiation

Figure 39 shows the VBG diffraction efficiency spectrum for three different cases. The diffraction efficiency spectrum of the grating at room temperature with no illumination by a high power radiation is shown by blue dots. Next, the heater temperature is set to 70° C, and the VBG is aligned with a low power beam. The dashed line in Figure 39 shows the diffraction efficiency for this condition. Next the high power beam is turned on, and the heater temperature is lowered until peak diffraction efficiency is recovered to its previous position. The diffraction efficiency of a probe beam produced by a VBG under exposure to the high power beam is measured and determined to be equal to that of the low power beam. The solid line shows the diffraction efficiency spectrum of the VBG with the high power beam turned on and the heater temperature

set to 55° C. The two curves overlap, demonstrating the conservation of resonance wavelength from low to high laser power.

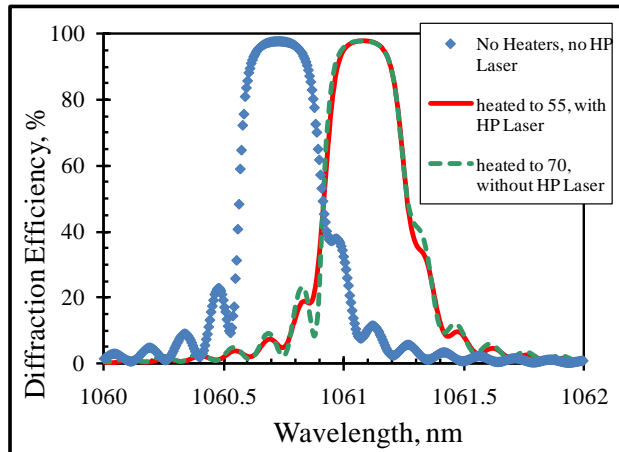


Figure 39: Diffraction efficiency under various heating conditions

Using this thermal tuning apparatus, the laser heats the glass from the center while the glass temperature is controlled from the edge. Without the use of thermal control, the temperature at the edge of a VBG under high power laser radiation is much cooler than the temperature at the peak of radiation. This thermal gradient produces a gradient in the Bragg wavelength of the VBG which can reduce combining efficiency. By heating the edge of the grating while high power radiation heats the center, the combined thermal gradient will be smaller than it would be without thermal control.

In order to examine the thermal profile across a VBG that has controlled edge temperatures with and without high power laser radiation heating a test beam is used to probe the resonant Bragg wavelength at various points across the aperture. A change in Bragg wavelength in this case is the result of expansion or contraction of the VBG and the associated Bragg period at the location of the test beam.

The experimental setup in Figure 38 is modified by replacing the low power output colimator which produces a 6 mm beam with one which produces a 3 mm beam. With a smaller test beam, different parts of the VBG can be probed more accurately.

Figure 40 shows the Bragg wavelength shift as a result of heating across the grating aperture while the VBG is under various heating conditions. The Bragg wavelength shift is the difference between the Bragg wavelength of the VBG at room temperature and under some external heating.

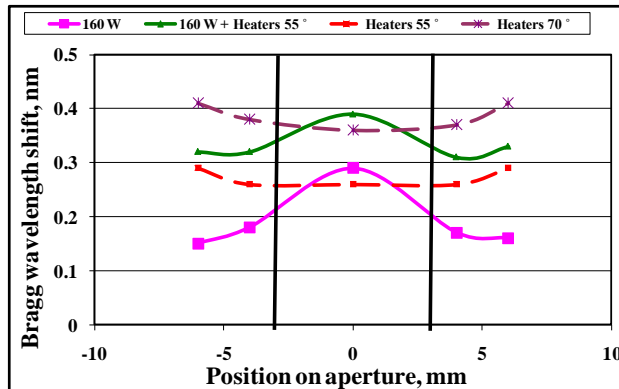


Figure 40: Bragg wavelength profile across the aperture under various heating conditions

The lower solid pink line shows the Bragg shift as a result of heating from only the laser source. Next the grating is pre-heated to a desirable starting temperature. The upper dashed line shows the Bragg wavelength profile while being heated from the edge to 70°C. When the laser radiation is turned on, the VBG edge temperature is reduced to 55°C. The Bragg wavelength profile that results from both high power laser radiation and heating at the edge is shown by the upper solid line (green). The Bragg wavelength gradient between the center and the edge of the VBG is significantly reduced in this case. Also, the resulting central Bragg wavelength is very near the intended central Bragg wavelength, and therefore diffraction efficiency is maintained without angle tuning the grating or spectrally tuning the laser.

The temperature of 55° C was found by lowering the temperature from 70° C until peak diffraction efficiency was restored. However, this temperature returned the central Bragg wavelength to just above the original Bragg wavelength associated with heating to 70°C without

the high power laser. This is a result of the Gaussian-like thermal profile the beam produces. The average deviation from this central wavelength from the edge of the beam to the center is minimized to achieve peak diffractin efficiency. Figure 41 illustrates this effect.

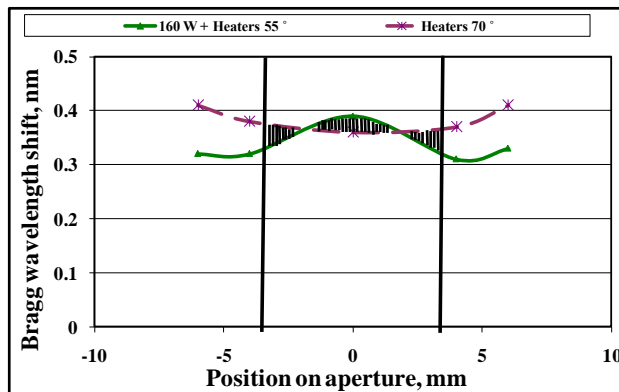


Figure 41: Profiles of deviation from initial Bragg wavelength for external heating to 70°C and a combination of external heating to 55°C and 160 W laser radiation

The beam quality of the test beam was measured to determine any effect the thermal tuning apparatus may have. Table 2 below shows the peak diffraction efficiency and M^2 under various heating conditions. It is clear from these results that the thermal tuning method does not deteriorate beam quality. The first three rows are the results of changing the VBG edge temperature without any high power radiation, while the final two rows show the results with high power radiation at two different VBG edge temperatures. In all cases, $M^2 \leq 1.12$, and diffraction efficiency was near 98%. For the case of using a high power beam without any

thermal control of the VBG, row four, the diffraction efficiency dropped down to 97.7%. This is the case associated with the highest thermal gradient across the aperture of the beam. The final case, row five, using high power radiation and thermal control of the VBG, reduces the thermal gradient and returns the diffraction efficiency to 98%.

Table 2: Diffraction efficiency and M^2 under various heating conditions

Incident optical power	Edge Temperature	Diffraction Efficiency	Test Beam M2
0 W	~25° (heater off)	98.0%	1.12
0 W	70° (heater on)	98.0%	1.09
0 W	55° (heater on)	98.0%	1.10
160 W	~37° (heater off)	97.7%	1.12
160 W	55° (heater on)	98.0%	1.09

In a spectral beam combining system, each beam in the SBC system will experience interaction with a different combination of VBGs as shown in Figure 15. The first beam transmits through four VBGs, while the second beam diffracts from one VBG and transmits through three, etc. Furthermore, each VBG is under a different thermal load. The first VBG experiences 150 W of power transmitting through it, and 150 W of power diffracting from it. While the second VBG experiences 300 W of power transmitting through it, as well as the same 150 W of diffracted power, etc. This is important because PTR glass has a small but finite

absorption. It means that the glass is heated under high power laser radiation, which causes glass expansion and refractive index change resulting in Bragg wavelength shift and thermal lensing. It is clear that each VBG experiences different heating conditions and therefore have a different Bragg wavelength shift. This shift is corrected by thermal tuning.

7 TESTING OF VOLUME BRAGG GRATINGS FOR HIGH POWER SPECTRAL BEAM COMBINING

7.1 Testing Diffraction Efficiency and Absolute Losses

Some special considerations must be made with testing volume Bragg gratings (VBGs) to be used in high power spectral beam combining (SBC). For the five beam design that is under consideration in this dissertation in which it is necessary to maintain high beam quality and total system efficiency of greater than 90 %, it is important that the peak in diffraction efficiency at the Bragg wavelength be greater than 98 %, and that the diffraction loss at the transmission wavelength be less than 3 %. Initial validation of a particular VBG starts with measuring the relative diffraction efficiency at the Bragg wavelength and at the nearest transmission wavelength of a desired spectral separation. A schematic of the testing setup used for this measurement is shown in Figure 42. In this simple configuration, a collimated and tunable laser beam is incident on a VBG such that the diffracted beam is measured by one detector while another measures the non-diffracted transmitting beam. The relative diffraction efficiency for the Bragg wavelength is determined by dividing the power at the diffracted detector by the sum of the powers at the diffracted and transmitting detectors. Similarly, relative transmission efficiency at the transmission wavelength is determined by dividing the power at the transmission detector by the sum of the power at the diffraction and transmission detectors.

When the VBGs for this project were delivered they were a full 40x40 mm in size, but the desired size was approximately 21x21 mm with a 12 mm diameter clear aperture in the

center. The full size pieces needed to be cut at the best location. For this reason, each VBG sample was placed on a stage with at least 40 mm of travel in the horizontal and vertical direction. In this way the VBG could be translated and tested until the best location is found. After finding locations of the full size sample which had acceptable diffraction efficiency, the beam quality of a beam diffracting from that location would need to be found, which will be discussed in the next section.

Absolute losses, must also be considered, and should be less than 1 %. Losses are typically measured at a wavelength far from the resonant Bragg wavelength to avoid any difficulty in measurement that may occur as a result of interaction with the grating. All the VBGs used in the project reported here had less than 1 % loss when measured far from resonance. The measurement setup is the same as in Figure 42. The measurement is accomplished by measuring the power of the input beam without any sample in the path. After which a VBG is placed in the beam path with the surface reflections being collected by the “diffraction” detector. The sum of the two detectors is divided by the power measured when no sample was present to determine the absolute efficiency.

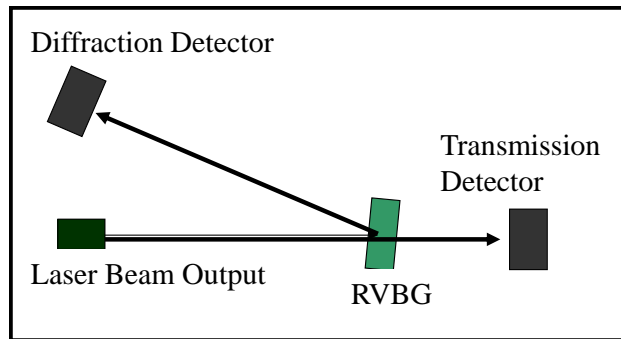


Figure 42: Relative diffraction efficiency test setup

Measuring for losses near the Bragg condition as a function of wavelength has produced some interesting results, specifically, that the losses in a given VBG are a function of detuning from the Bragg condition. A model to describe these losses as a function of detuning from the Bragg condition has been developed by a research colleague⁷⁸.

A test setup capable of measuring both relative and absolute diffraction efficiency as a function of wavelength was designed and built. A schematic of this setup is shown in Figure 43. The absolute loss setup is similar to the setup used for relative diffraction efficiency except that a beam wedge is placed in the beam path just after the laser source such that the results measured from the transmission and diffraction detectors can be normalized to the sampled input beam power. For a lossless system, the sum of the transmitted and diffracted beams from the VBG should have a constant ratio with the sampled input beam. Any reductions in total measured power divided by the sampled input power indicates scattering or absorption loss. A typical plot

of the losses in a VBG as a function of wavelength near the Bragg condition is shown in Figure 44.

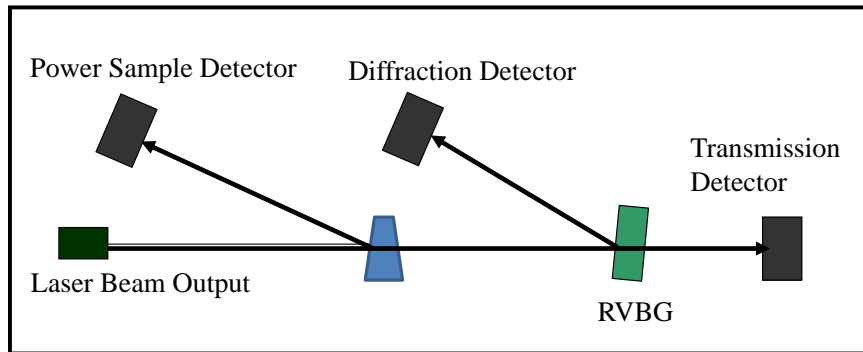


Figure 43: Absolute efficiency and loss test setup

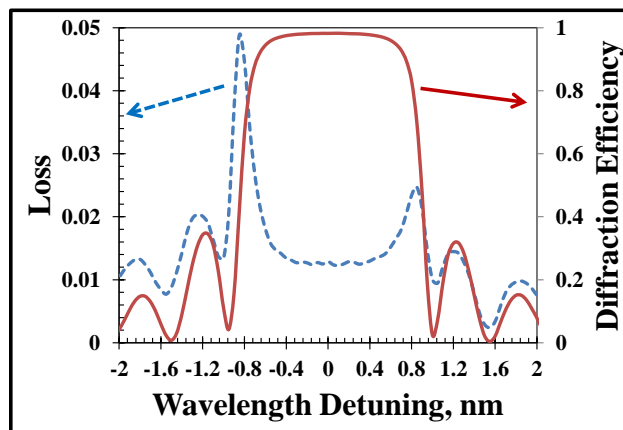


Figure 44: Typical result from absolute efficiency and loss measurement

The features of this plot show a correlation between the periodic structure of the VBG side lobes and the peak in diffraction losses. The losses reach a peak very near, but not exactly at, the first minimum in diffraction efficiency of the VBG. This behavior can be explained by considering that the optical intensity profile inside the VBG when interacting with the VBG varies with detuning from resonance. At the first minimum of diffraction efficiency, the VBG behaves like a resonant cavity in which the power constructively interferes in the forward propagating direction, and hence the optical intensity inside the VBG is significantly higher than it is far from resonance. At Bragg resonance, the losses are seen to fall significantly from the peak. This is due to the fact that at resonance the total optical intensity inside the VBG decays exponentially from the surface of the VBG. Far from resonance the power through the VBG should be nearly flat with only material losses diminishing the initial power.

7.2 Testing for Beam Quality, Astigmatism and Defocus of a Diffracted Beam

After a VBG has been identified which has the proper diffraction efficiency and loss requirements, it is equally important to test the characteristics of a beam that is diffracted from the VBG. Inhomogeneity or defects in the glass can cause random distortions in a diffracted beam which will decrease its beam quality. Also, a holographically recorded VBG can be slightly curved inside the glass. This can cause defocus or astigmatism in a diffracted beam. Defocus in a single beam is not a significant issue as this does not affect beam quality. However, as discussed in chapter 5, if multiple beams are co-propagating and have defocus greater than $\frac{1}{2}$ of the Rayleigh length, the combined beam quality will be reduced.

Astigmatism, besides reducing beam quality within a single beam can cause an additional problem when using the beam for SBC. As discussed in detail in chapter 5, the final step in aligning a high power VBG based SBC system is to align the beam waists of the individual beams. If astigmatism is present in some or all of the beams, the beam waists for the horizontal plane and vertical plane will be in different locations. When aligning the beam waists, one plane must be chosen for alignment, and the waists in the other plane will fall randomly around the focus depending on the particular astigmatism of each individual beam.

The setup used is the same as in Figure 42, except that the diffraction detector is replaced with a lens and a Beam Map device which can measure both the beam quality, and beam waist location of any beam or beams sent through its associated lens in both the horizontal and vertical planes. The focal length of this lens depends on the input beam size and typically a 50 to 100 mm lens is used. The Beam Map devices measures the intensity cross section of the focusing beam at five different planes spaced by about 500 μm in the propagation direction. From this cross section the 2nd moment beam diameter is calculated and the M^2 of the beam is calculated.

The Beam Map must first be calibrated by finding the beam waist location of an ideal Gaussian beam. An ideally collimated Gaussian beam with $M^2 = 1$ is sent into the Beam map device, and the absolute location of the beam waist of this beam is noted.

In order to test a particular VBG, an ideally collimated Gaussian beam with $M^2 = 1$ is diffracted from the VBG and sent into the beam map. The M^2 , and the beam waist location in

both the horizontal and vertical planes are measured relative to the ideal beam waist location. Ideally, the $M^2 = 1$, and the defocus in both planes is zero. However, most good VBGs degrade the beam quality of an ideal beam to $M^2 = 1.1 - 1.15$, and most good VBGs have some defocus and astigmatism. As discussed, above, VBGs were chosen for this project for which the defocus and astigmatism was less than $\frac{1}{2}$ of the Rayleigh Length.

8 HIGH POWER SBC OF FIBER LASERS WITH ULTRA HIGH SPECTRAL DENSITY

8.1 Two Beam Experiments

The novel thermal tuning technique, previously described in detail, can be used in spectral beam combining to keep the gratings in resonance from low power up to the full power of a given SBC system. Formerly, a SBC system would be aligned such that peak combining efficiency is achieved only after the VBGs heat up under high power laser radiation and reach thermal equilibrium. In this case, any fine tuning of the system would require angular adjustments to the VBGs while maintaining full input laser power. Angle tuning a VBG while kW-level radiation is incident on the grating is impractical. Thermal tuning eliminates the need for mechanical tuning and may be electronically controlled with proper feedback. Mechanical alignment is used only to make each beam co-linear, while thermal tuning is used to maintain peak combining efficiency throughout the power range of the system.

Figure 45 shows the experimental setup for 2 channel high power spectral beam combining. One VBG with thermal tuning is used to combine two high power lasers. Figure 46 shows the optimal VBG edge temperature as a function of power level. The combining efficiency for each data point is also given. From 10 W to over 300 W, beam combining efficiency was maintained constant within 0.5% of the low power combining efficiency. No angular tuning was required to maintain the combining efficiency.

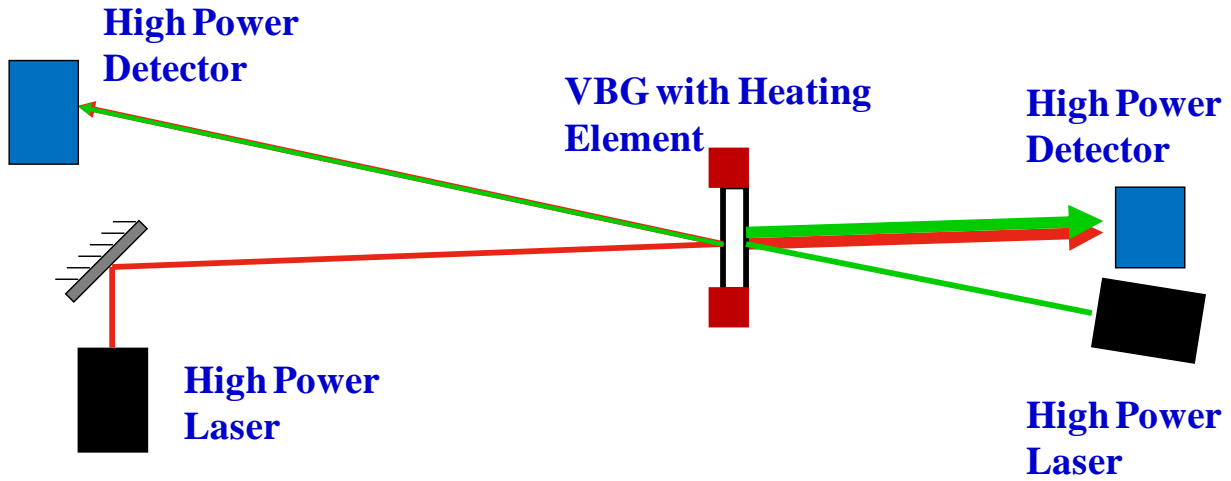


Figure 45: Two channel high power SBC experimental setup

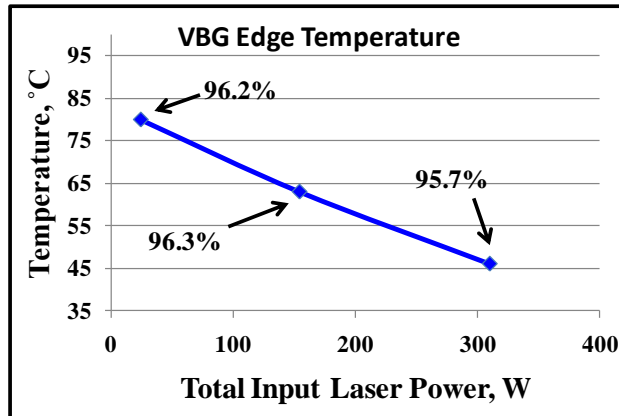


Figure 46: Two channel beam combining efficiency at different power levels and VBG edge temperatures

The M2 beam quality factor for two channel SBC at 300 W was measured to be $M_x^2 = 1.19$, and $M_y^2 = 1.16$, while the M^2 of the individual beams was measured to be less than 1.05.

Figure 47 shows the combined results for the vertical case. The device used to measure M^2 is rated to be accurate to $\pm 10\%$. The radiance of the combined beam is calculated to be, $180 \frac{TW}{(sr*M^2)}$. The individual beams had a radiance of $120 \frac{TW}{(sr*M^2)}$. This gives a BCF of 0.75. The total spectral bandwidth of the combined beam is 0.25 nm, therefore the spectral radiance is calculated to be $719 \frac{TW}{(sr*M^2*nm)}$. To my knowledge, this is the highest spectral radiance for any spectral beam combining system demonstrated to date.

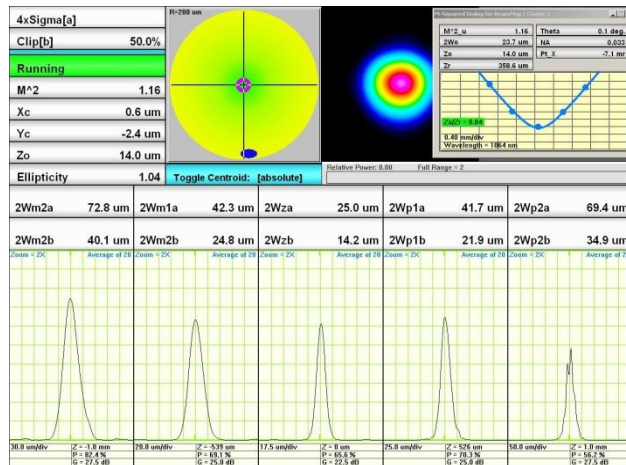


Figure 47: 2-Beam, 300 W, SBC M^2

8.2 Five Beam Experiments

8.2.1 Ultra High Density SBC with Low Power Beams

The thermal tuning setup was expanded to 5 channels. Low power, less than 1 W, experiments resulted in a total combining efficiency for 5 channels was greater than 90%, and combined beam $M^2 < 1.1$, and BCF of 0.76 has been demonstrated. Figure 48 shows the beam quality test results for 5 combined low power beams. The 5 channel results were completed using high quality low power input beams.

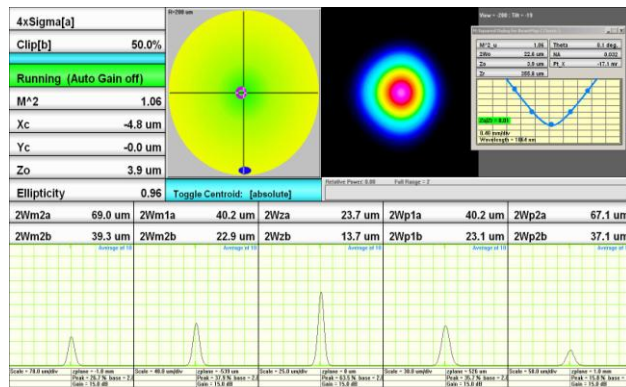


Figure 48: Five channel, combined low power beam quality, $M^2=1.06$

After completing the low power tests, the SBC system was adapted to be used with 5 high quality ($M^2 < 1.2$), high power beams, and 0.75 kW output within 1 nm using thermally tuned VBGs was demonstrated. The system is designed to be aligned at low power and temperature tuned for uninterrupted operation at any power up to the maximum. The result

shows the highest power spectral density to date, 0.75 kW/nm, of any spectral beam combining system.

Five 150 W beams were combined in the architecture shown in Figure 15. Efficiency of greater than 90 % was maintained from 75 W to 750 W total power.

The VBGs used in this experiment have absorption in the range of $\alpha = 1-2 \times 10^{-3} \text{ cm}^{-1}$. The relationship between the optical power absorbed in the VBG and the absorption coefficient is given by, $I_{abs} = I_0(1 - 10^{-\alpha L})$.

The beams were first aligned to operate at 20 W each, 100 W total. The beam quality of each beam was measured after passing through the beam combining system and the measured M^2 value for beams one through five are 1.22, 1.23, 1.27, 1.08, and 1.05, and the combined beam quality was measured to be $M^2 = 1.20$, where beam one transmits through all VBGs and beam five is diffracted off of the final VBG and does not transmit through any. Figure 49 shows the combined beam quality measurement for the case of 100 W total power. From Figure 31, in the case of five beams with $M^2 = 1.2$, it can be seen that this results in an increase of radiance over that of a unit beam of approximately 3.5 times, and the BCF is calculated to be 0.77.

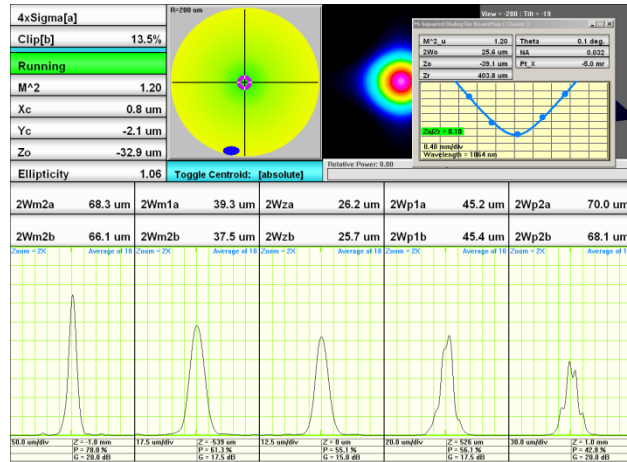


Figure 49: Quality of a combined beam in the five beam 100 W SBC system, 20 W each beam.

8.2.2 Ultra High Density, High Power SBC with High Absorption VBGs

For the case of 750 W total power, the beam quality of each individual beam was measured while the system was operating at full power by using the demultiplexing measurement setup described above and shown in Figure 34. The individual beams, one through five, after passing through the system were found to have M^2 of 3.15, 2.82, 2.74, 1.77, and 1.36 respectively. The combined beam quality before alignment of the beam divergences was measured to be $M^2 = 3.0$, and after alignment of the beam divergences, the combined beam quality was reduced to $M^2 = 2.1$. The resulting spectral radiance is calculated to be $138 \frac{TW}{sr \cdot m^2}$, the highest to date for any five beam SBC system. From Figure 31, in the case of five beams with $M^2 = 2.1$, it can be seen that this results in an increase of radiance over that of a unit beam of only 1.13 times, and the BCF is calculated to be 0.25.

To confirm the beam combining model described above, as well as the measured result of $M^2 = 2.1$, the measured M^2 values for each beam were used as inputs to calculate the expected combined beam quality. The model shows that combining five beams with beam quality factors, M^2 , of 3.15, 2.82, 2.74, 1.77, and 1.36, gives an expected combined beam quality of $M^2 = 2.04$ after considering the additional effect on beam quality of the demultiplexing VBG. This calculated result is very close to the measured result of $M^2 = 2.09$ shown in Figure 50. It can be concluded that the beams are co-propagating and the beam divergences are well aligned. The model also confirms the low power result with the calculated combined beam quality factor $M^2 = 1.17$ being very close to the measured result of $M^2 = 1.20$.

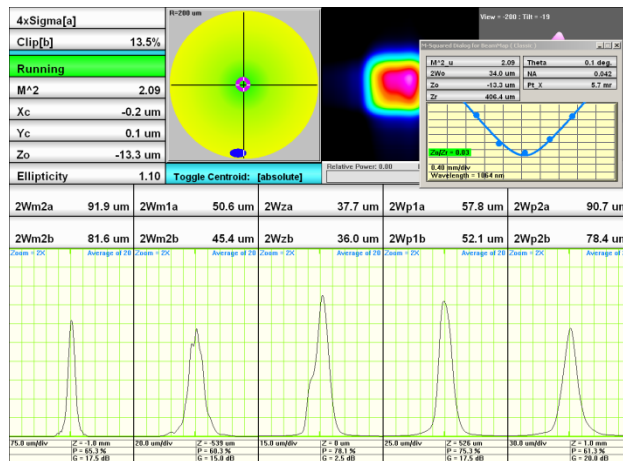


Figure 50: Combined beam quality of the five beam 750 W SBC system using interim VBGs

An experiment was conducted in order to determine if the controlled edge temperature of the final VBG is contributing to a thermal gradient that reduces beam quality. The final VBG in the system is heated from the center by 600 W of laser power transmitting through the grating. In this experiment the final diffracting beam in the system is turned off for reasons that will become clear later. The center temperature while in resonance is near 71° C, while the edge temperature is near 40° C. To determine if the controlled edge temperature contributes to a thermal gradient that may reduce beam quality, the edge temperature is gradually increased up to 80° C. The combined beam quality of the transmitting beams is measured at various temperatures. If the relatively low temperature of the edge of the VBG as compared to the center is contributing to beam quality degradation, it is expected that the beam quality of the transmitting beams would improve during the heating process. It is found that the combined beam quality remains unchanged from 40° C to 80° C, which suggests that the thermal gradient produced by laser induced heating near the center of the VBG is negligibly effected by the temperature at the edge of the VBG. Therefore, this thermal tuning technique can be used in high power applications without adversely affecting beam quality.

8.2.3 Ultra High Density, High Power SBC with Low Absorption VBGs

The exact same setup from the previous section is used with the same lasers but with lower absorption VBGs. PTR glass can be manufactured with absorption as low as $\alpha = 1 \times 10^{-4} \text{ cm}^{-1}$, but the VBGs that were delivered for the final stage of this project were tested to have absorption of $\alpha = 2-4 \times 10^{-4} \text{ cm}^{-1}$.

The specifications for various parameters of interest for each of the VBGs used in this final demonstration are given in Table 3. VBG 1 is the grating which first in the system with respect to the beam propagation direction. VBG 4 is the final grating through which four beams are transmitted and one is diffracted. The Relative DE at λ_B is the diffraction efficiency of the VBG at the Bragg wavelength, while the Relative DE at λ_T is the diffraction loss at the nearest transmission wavelength. Material losses were tested far from resonance at 1070 nm. In VBG 3 the astigmatism is larger than the ideal half of the Rayleigh length, but this grating was chosen due to its excellent performance with regard to its other properties. The same is true with respect to VBG 4 and its defocus.

Table 3: Summary of VBG properties

	VBG 1	VBG 2	VBG 3	VBG 4
Designation	C25-04	C25-02	C25-09	C25-10
M2-horizontal	1.08	1.09	1.08	1.03
M2-vertical	1.03	1.06	1.10	1.06
Relative DE at λ_B	99.20%	98.00%	98.58	98.10%
Relative DE at λ_T	5.10%	3.00%	2.43%	2.75%
Spectral Separation (nm)	0.25	0.25	0.248	0.25
Material Loss (1070 nm)	0.9%	< 1 %	< 1 %	0.82%
Astigmatism (Dz/Zr)	0	0.02	1.23	0.12
Defocus (Dz/Zr)	0	0.19	0	1.06

The full power, 750 W SBC system was re-aligned with the lower absorption VBGs. The combined output power was 685 W. The spectral separation between beams was less than 0.25 nm, efficiency was 90.5 % and $M^2 = 1.5$ was achieved after alignment of the beam waists. The final result and record for spectral radiance in any high power multi-beam SBC system is $783 \frac{TW}{sr \cdot m^2 \cdot nm}$, and $270 \frac{TW}{sr \cdot m^2 \cdot nm}$ for the two and five beam cases respectively.

Each VBG in the system was aligned at low power to operate with an edge temperature of 70 °C for VBGs one through three, and the final VBG was set to an edge temperature of 80 °C. As seen in chapter 0, the temperature difference between the edge and the center of the VBG when heated from the edges is between 8 and 9 °C when there is no high power beam present. So, it is expected that even with 600 W transmitting through the final VBG and 150 W diffracting from it, the temperature in the center of the VBG should be around 72 °C if resonance is to be maintained. Figure 51 shows the thermal profile of the final VBG while operating at full power. The peak temperature is shown to be about 74 °C which indicates a slight thermal gradient in which the center of the VBG is slightly above the initial resonant temperature. This behavior is also expected as discussed in chapter 0.

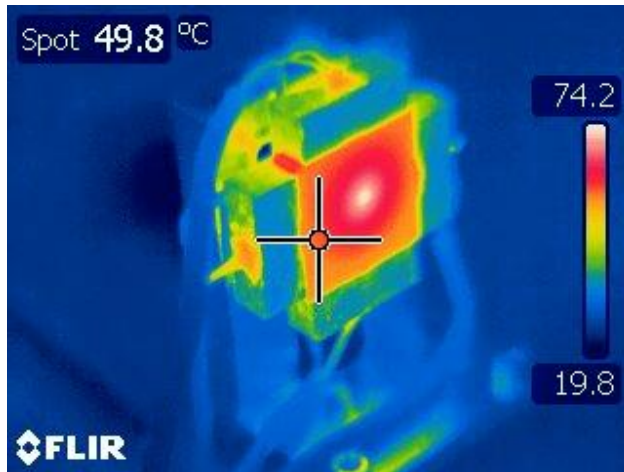


Figure 51: Thermo image of last VBG from lower absorption VBG set in the five beam 750 W spectral combiner.

Figure 52 shows the final SBC setup operating at full power. The spectrum is shown in Figure 53, and Figure 54 shows the final beam quality measurement in the vertical direction.

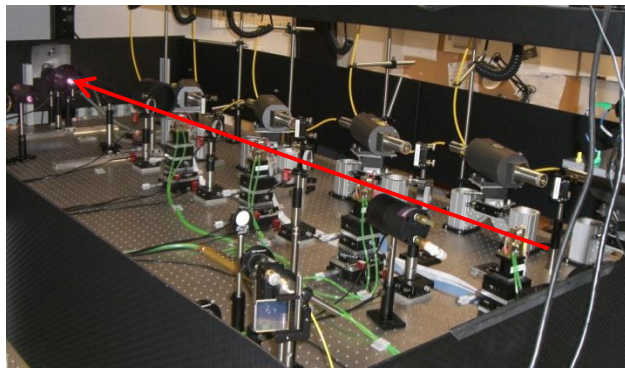


Figure 52: Photo of experimental setup with beam propagating from right to left.

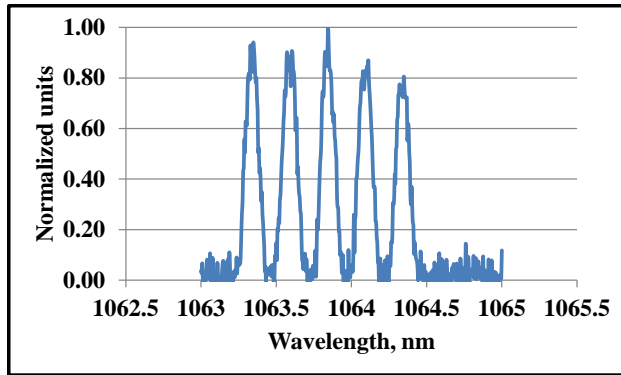


Figure 53: Combined spectrum of 750 W SBC system

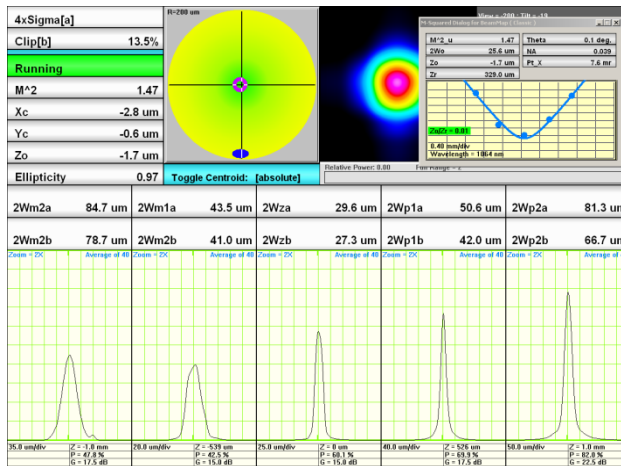


Figure 54: Combined beam quality of the five beam 750 W SBC system using final low absorption VBGs

8.3 Wavelength, and Pointing Stability of Lasers

The lasers used in the high power experiments necessarily must have high pointing stability, and high wavelength stability. As discussed in the thermal tuning section of this work, the transmitting beam which is nearest in wavelength to the diffracting beam is only 45 pm from

the nearest local maximum in diffraction efficiency. This is illustrated in Figure 36. For this reason the wavelength stability of the laser is very important. To be effective, the laser wavelength must be stable to within a few picometers. Figure 55 shows the long term wavelength stability the laser. Over a period of one hour, the wavelength deviation was approximately ± 0.002 nm from the average. This is well within a reasonable tolerance as the maximum deviation of 0.004 nm is less than 10 % of the distance from the local minimum to local maximum illustrated in Figure 36. It is worth noting that the optical spectrum analyzer used to measure the data is rated for wavelength measurement stability of ± 0.005 nm.

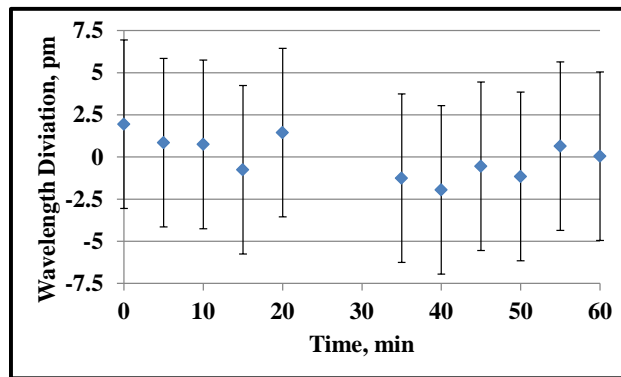


Figure 55: Long term wavelength stability of high power fiber lasers.

Also important is the pointing stability of the laser, that is to say, the stability of the angular position of the beam. This is significantly more important for beam combining than many other laser applications due to the fact that all five beams must be co-propagating for the

resulting combined beam to show high radiance at a focal spot or on a target at a distance. The effect of pointing stability can be seen in the measurements for beam quality, and so does not necessarily need to be explicitly given. However, to be thorough it is given here. Figure 56 shows a plot of the measured focus locations of the laser after a 50 mm lens over a nearly two hour period. The red dot at (0,0) represents the centroid of the data set. The size of the beam at the focus is approximately 20 μm . The standard deviation in position on the focal plane is approximately 0.62 μm , which translates to 12.4 μrad in angle. The diffraction limited divergence of the 6 mm diameter beam is 112 μrad . The pointing error is approximately 11 % of the diffraction limited divergence. This small pointing error is within a reasonable margin for SBC which is verified by the high beam quality from both the low power and high power SBC experiments. Figure 57 shows a points in the bucket curve. The ratio of points that falls within a given radius is plotted as a function of radius. The vertical line of Figure 57, and the circle of Figure 56 both represent the radius within which 90 % of the data points fall.

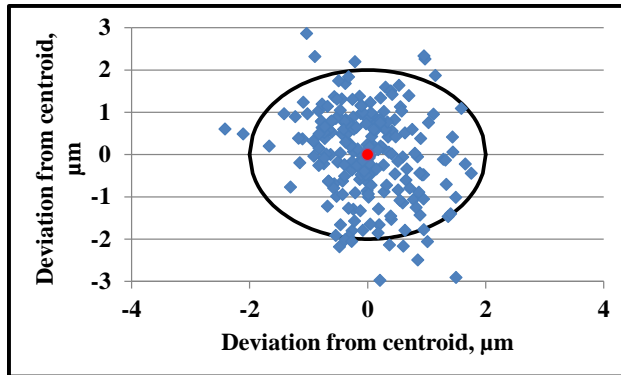


Figure 56: Long term (1hr 45min) pointing stability of high power fiber lasers after 50 mm lens. Standard deviation in focal position = $0.62 \mu\text{m}$, which translates to $12.4 \mu\text{rad}$ in angle. The half-angle diffraction limited divergence for the 6 mm diameter beam is $112 \mu\text{rad}$.

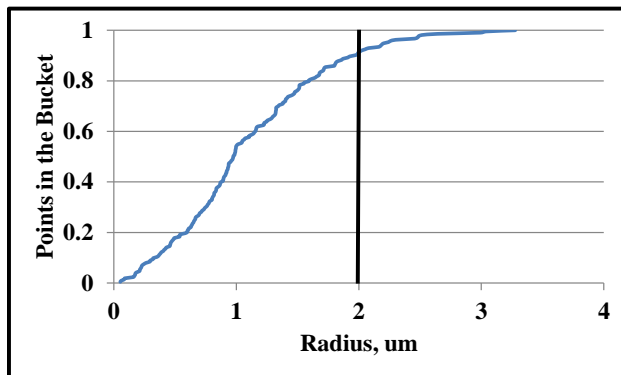


Figure 57: Long term (1hr 45min) points in the bucket curve based on the data from Figure 56. The plot shows the ratio of points (vertical-axis) that fall within a given radius (horizontal-axis).

9 FUTURE DIRECTIONS FOR RESEARCH IN VBG-BASED SBC

9.1 Spectral Beam Combining by Multiplexed Volume Bragg Gratings

For practical and perhaps mobile use of such beam combining systems, a more compact architecture is desirable. A new architecture for SBC with multiple VBGs recorded into a single piece of PTR glass is demonstrated which significantly reduces the footprint of the spectral beam combiner. In previous architectures, each beam combining element would diffract a single beam into the common beam path, while other beams would transmit through an individual element. For this new architecture, multiple VBGs have been recorded into one PTR glass sample. For each VBG recorded into the glass, one laser beam can be diffracted from it allowing each beam combining element to diffract multiple beams into the common beam path, illustrated in Figure 58. A spectral beam combiner based on multiplexed VBGs is reported⁷⁹.

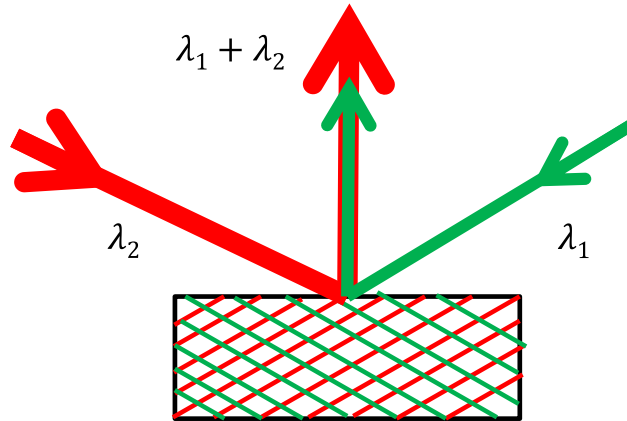


Figure 58: Multiplexed spectral beam combining geometry⁷⁹.

As discussed in previous chapters of this dissertation, thermally induced heating of VBGs have resulted in a thermal shift of the Bragg wavelength, thermally induced degradation of beam quality, and thermally induced lensing. It is clear from the high power high absorption results reported in section 8.2.2 that the final diffracted beam has very little beam quality degradation as a result of being diffracted from the final VBG, even though the final VBG has the highest thermal load. It is the successive transmission of the first beam through multiple VBGs which causes the highest degradation in beam quality. By recording multiple VBGs in the same piece of PTR glass. Each beam can be diffracted in a single stage SBC architecture. The two beam example is shown in Figure 58.

Low power SBC by a multiplexed VBG for two beams has been demonstrated with relative efficiency of 98 %, and $M^2 < 1.1$. The beam quality results are shown in Figure 59.

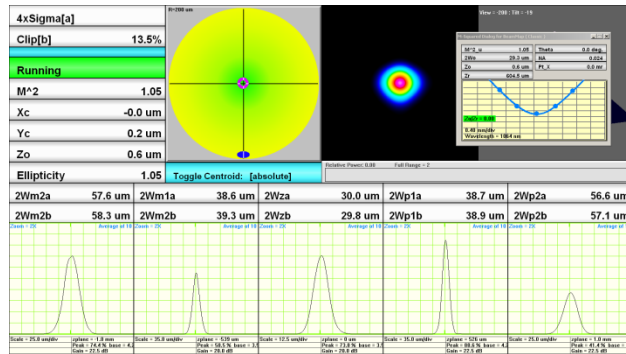


Figure 59: Combined M^2 for SBC of two beams by multiplexed VBGs

It is important to point out the importance of maintaining control of the Bragg resonance when using this architecture with high power beams. Even though PTR glass has very low absorption and diffracting beams do not induce the level of distortion that transmitting beams do, it is clear that thermal expansion of a multiplexed VBG will still shift the Bragg wavelengths. Two possible methods of controlling this are to adjust the wavelength of the lasers in use as the VBGs heat up, or to maintain thermal control of the VBGs. One of these two methods would need to be implemented in any multi-kW SBC system based on multiplexed VBGs.

This method of spectral beam combining by multiplexed VBGs is still under investigation. It is still not clear how many VBGs with high diffraction efficiency can be

practically recorded into a single piece of low loss PTR glass. New samples are expected to be available in the near future for further experiments at high power and with greater than two beams.

9.2 Beam Quality Improvement with Flat Top Heating Profile

Beam quality degradation in the final high power SBC system is due to thermally induced distortions in the PTR glass. Laser heating of the glass in a Gaussian profile causes both thermal lensing and additional higher order aberrations. The thermal lensing is corrected by adjusting the collimation of each beam at the input such that the output divergences are equal. In this way the spherical component to the thermally induced lens is corrected. This effect has been discussed in more detail chapter 5.

It has been proposed that utilizing a super Gaussian beam rather than a Gaussian beam will improve the beam quality of high power beams transmitting through the glass⁸⁰. In a proposed 100 kW system, high speed gas flow cooling will be required to keep the VBGs below 200 °C. This high speed cooling will also cause the thermal profile across the aperture of the glass to mirror the intensity profile of the beam heating the glass. Modeling of this effect by a fellow graduate student, Sergiy Mokhov, in Dr. Zeldovich's group reveals the implications of this concept.

Figure 60 shows the calculated beam quality as a function of phase shift in the glass for both the Gaussian and super Gaussian cases. The phase shift is caused by high power incident

laser radiation and therefore glass expansion. Utilizing a super Gaussian rather than a Gaussian beam causes the phase shift across the aperture of the beam to have a flat top shape rather than a Gaussian shape. This reduces the distortion introduced into a transmitting beam and the beam quality remains high even at very high optical powers.

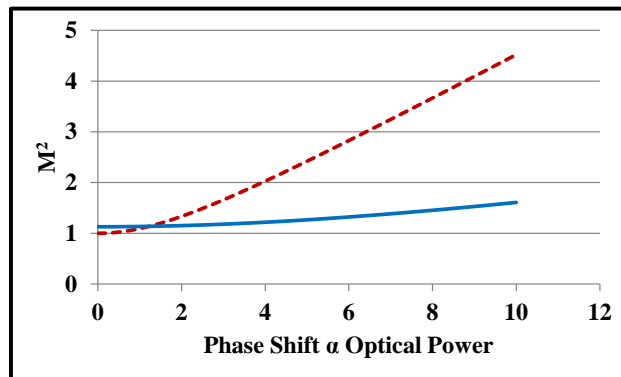


Figure 60: Calculated M^2 for Gaussian (dashed line) and super Gaussian (solid line) high power beams transmitting through as a function of phase shift where phase shift is proportional to incident laser power at glass absorption⁸⁰.

Although the high speed gas cooling has not yet been implemented, an experiment has been performed to verify this behavior. Figure 61 shows a schematic of the experimental setup used to compare beam quality degradation in a transmitting beam with a Gaussian vs. a flat top profile.

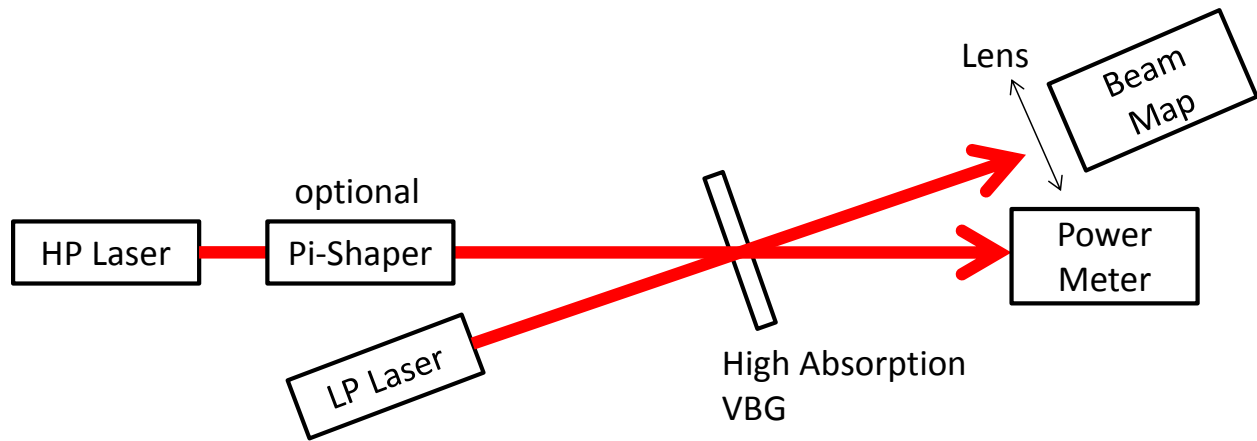


Figure 61: Experimental setup to measure M^2 for Gaussian (without pi-shaper) and super Gaussian (with pi-shaper) high power laser beams.

For this experiment, a very high absorption VBG is used with absorption of $\alpha=1.65 \times 10^{-2}$. This absorption is 165 times higher than the state of the art absorption of $\alpha = 1 \times 10^{-4}$. So the power used in this experiment is simulating the effect in state of the art low absorption glass of a beam with 165 times higher power. The reported power is the simulated laser power, 165 times higher than the actual power used.

The high power beam in this experiment is used only as a heater, while a test beam is propagated through the VBG and overlapping with the high power beam at the VBG. Any distortions caused by the high power beam will affect the beam quality of the low power beam as it transmits through the same piece of high absorption PTR glass. This low power test beam is then measured for beam quality at each power level to determine the distortion. After conducting the experiment with a Gaussian beam, a pi-shaper is used to convert the Gaussian

beam to a nearly flat top beam which is then used as a heater to repeat the same experiment. Figure 62 shows the measured beam quality degradation in the low power test beam with increased high power laser heating for both cases. Although there is not a dramatic difference in beam quality between the two experiments, there is a clear improvement when using the flat top beam as a heater.

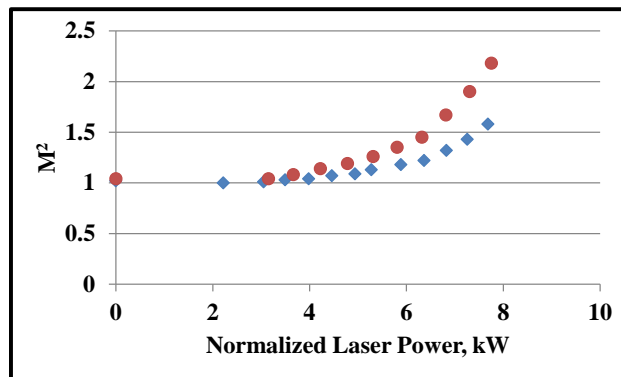


Figure 62: Measured M^2 for Gaussian (Circles) and super Gaussian (Diamonds) high power beams transmitting through high absorption PTR glass as a function of normalized incident laser power.

The dramatic improvement that was predicted in Figure 60 is due to the fact that the calculation assumes very high speed gas cooling of the glass surface. This causes the thermal profile to be more dramatic than in the case of this experiment in which much of the heat diffuses in the glass causing a softening of the thermal profile.

It is clear from this result, that reduced thermal distortions can be achieved by utilizing a super Gaussian instead of a Gaussian beam when high power lasers are transmitting through absorbing glass.

10 CONCLUSIONS

High radiance fiber laser sources are becoming available, but non-linear and thermal effects still limit their peak power. Laser systems with 100 kW level diffraction limited output remain elusive. Beam combining techniques such as coherent phased array and incoherent spectral beam combining are being employed to increase the laser system radiance and hopefully achieve ultra-high radiance. Coherent beam combining has had significant success, boasting the highest power beam combining system, with 100 kW of output power, but poor beam quality reduces the radiance of the system to $11,028 \frac{TW}{sr*m^2}$, which is less than that of a single 15 kW input beam with diffraction limited divergence. Spectral beam combining by surface diffraction gratings has been very popular, and is still achieving incremental success with up to 2 kW of output power demonstrated with M^2 of 1.9, and bandwidth of 15 nm. This results in a radiance of $491 \frac{TW}{sr*m^2}$, but a spectral radiance of only $33 \frac{TW}{sr*m^2}$. Spectral beam combining by volume Bragg gratings has made significant progress in the last five years. A spectral separation of 0.25 nm between beams for high power, 750 W, five channel beam combining has been demonstrated, and near diffraction limited beam quality for this system is reported here. The resulting SBC system has an output power of 685 W, $M^2 < 1.5$, and a total bandwidth of 1 nm. The radiance is $270 \frac{TW}{sr*m^2}$ with a spectral radiance of $270 \frac{TW}{sr*m^2*nm}$. It is the youngest of the major methods, and has great potential to be the building block of ultra-high radiance laser systems.

1. A method of optimization of VBGs for SBC is developed. A method of including the effect of laser beam divergence and spectral bandwidth into the diffraction efficiency spectrum of a VBG has been presented, as well as an optimization method for determining the best VBG parameters in terms of thickness and refractive index modulation. It was presented that although an absolute maximum in efficiency can be achieved by using very thick VBGs that make use of a high order minimum in the diffraction efficiency spectrum for transmitting beams, there is little benefit in combining efficiency over using thinner VBGs that make use of the third minimum. The VBG optimization method was expanded to optimized full SBC systems with an arbitrary number of beams and VBGs for an arbitrary beam divergence, and spectral separation.
2. A model describing the effect of divergence of individual beams on the divergence of the combined beam is developed. A model to describe the combined beam quality of multiple beams with unique divergences and initial beam qualities has been developed. It is concluded that the divergence of ideal diffraction-limited beams can vary up to the point at which the beam waists are shifted by $\frac{1}{2}$ of a Rayleigh length before significant degradation of beam quality or combined beam radiance occurs.
3. The Beam Combining Factor (BCF) has been described in which the quality of beam combining can be determined without concern for the quality of the individual input beams. The BCF is a universal measure of quality of beam combining for any method of beam combining.

4. A method to control the divergence of individual beams by demultiplexing of the combined beam is developed. A novel demultiplexing apparatus and beam measurement system has been demonstrated and successfully used to measure and align the divergence of all five spectrally combined beams. At low power operation, 100 W total, the combined beam quality was measured to be $M^2 = 1.20$. In the case of full power operation, 750 W total, the alignment of the beam divergences resulted in the improvement of combined beam quality from $M^2 = 3.0$ to $M^2 = 2.1$, The calculated result of $M^2 = 2.04$ matches reasonably well with the measured result.
5. After utilizing low absorption VBGs with the same thermal tuning and waist alignment techniques, near diffraction limited beam quality with $M^2 = 1.5$ was demonstrated for a 750 W SBC system with 0.25 nm spectral separation between beams and greater than 90 % efficiency.
6. A method of thermal alignment of a beam combiner is proposed and implemented in the experimental setup. Volume Bragg grating thermal tuning devices were successfully employed to maintain diffraction efficiency above 90 % for the entire power range of a five beam 750 W spectral beam combining system with a spectral separation between beams of 0.25 nm, achieving, to the knowledge of the authors, the highest power spectral density of any spectral beam combining system to date of 0.75 kW/nm. The highest spectral radiance is also reported for both two beam and five beam SBC with $718.5 \frac{TW}{sr \cdot m^2 \cdot nm}$, and $270 \frac{TW}{sr \cdot m^2 \cdot nm}$ respectively.

7. Two beam spectral beam combining by a multiplexed volume Bragg gratings has been demonstrated with relative efficiency of 98 %, and $M^2 < 1.1$.
8. Reduction of thermal distortions in beams transmitting through high absorption PTR glass by use of a flat top beam in place of a Gaussian beam has been demonstrated.
9. The record highest spectral brightness achieved by spectral beam combining is demonstrated.

LIST OF REFERENCES

- ¹ T.Y. Fan, IEEE Journal of Selected Topics in Quantum Electronics **11**, 567-577 (2005).
- ² J. Limpert, F. Roser, S. Klingebiel, T. Schreiber, C. Wirth, T. Peschel, R. Eberhardt, and A. Tinnermann, IEEE Journal of Selected Topics in Quantum Electronics **13**, 537-545 (2007).
- ³ Jay W. Dawson, Michael J. Messerly, Raymond J. Beach, Miroslav Y. Shverdin, Eddy A. Stappaerts, Arun K. Sridharan, Paul H. Pax, John E. Heebner, Craig W. Siders, and C.P.J. Barty, Optics Express **16**, 13240 (2008).
- ⁴ J.R. Leger and W.C. Goltsov, IEEE Journal of Quantum Electronics **28**, 1088-1100 (1992).
- ⁵ Stark, L., Ieee **62**, 1661-1701 (1974).
- ⁶ José E. Ripper, Applied Physics Letters **17**, 371 (1970).
- ⁷ Stuart J. McNaught, Charles P. Asman, Hagop Injeyan, Andrew Jankevics, Adam M. Johnson, Gina C. Jones, Hiroshi Komine, Jason Machan, Jay Marmo, Michael McClellan, Randy Simpson, Jeff Sollee, Marcy M. Valley, Mark Weber, and S Benjamin. Weiss, in *Frontiers in Optics* (Optical Society of America, 2009), p. FThD2.
- ⁸ T. M. Shay, Vincent Benham, J. T. Baker, Benjamin Ward, Anthony D. Sanchez, Mark A. Culpepper, D. Pilkington, Justin Spring, Douglas J. Nelson, and Chunte A. Lu, Optics Express **14**, 12015 (2006).
- ⁹ Baishi Wang, Eric Mies, Monica Minden, and Anthony Sanchez, Solid State and Diode Laser Technology Review **1060**, 2-6 (2008).
- ¹⁰ Hans Bruesselbach, Monica Minden, Jeff L. Rogers, D C. Jones, and Metin S. Mangir, in *Conference on Lasers and Electro-Optics/Quantum Electronics and Laser Science and Photonic Applications Systems Technologies* (Optical Society of America, 2005), p. CMDD4.
- ¹¹ Akira Shirakawa, Keigo Matsuo, and Ken-ichi Ueda, in *Conference on Lasers and Electro-Optics/International Quantum Electronics Conference and Photonic Applications Systems Technologies* (Optical Society of America, 2004), p. CThGG2.

- ¹² Apurva Jain, Oleksiy Andrusyak, George Venus, Vadim Smirnov, and Leonid Glebov, Proc. of SPIE **7580**, 75801S-1-75801S-9 (2010).
- ¹³ Apurva Jain, Derrek Drachenberg, Oleksiy Andrusyak, George Venus, Vadim Smirnov, and Leonid Glebov, in *Laser Technology for Defense and Security VI*, edited by Mark Dubinskii and Stephen G. Post (SPIE, Orlando, Florida, USA, 2010), pp. 768615-8.
- ¹⁴ O.E. DeLange, in *Proceedings of the IEEE* (1970), pp. 1683-1690.
- ¹⁵ H. Ishio, J. Minowa, and K. Nosu, Lightwave Technology, Journal Of **2**, 448-463 (1984).
- ¹⁶ I.H. White, Journal of Lightwave Technology **9**, 893-899 (1991).
- ¹⁷ M.C. Farries, A.C. Carter, G.G. Jones, and I. Bennion, Electronics Letters **27**, 1498 (1991).
- ¹⁸ C.C. Cook and T.Y. Fan, in *Advanced Solid State Lasers*, edited by M. Fejer (Optical Society of America, 1999), p. PD5.
- ¹⁹ Erik J. Bochove and Craig A. Denman, in *Laser Resonators III*, edited by Alexis V. Kudryashov and Alan H. Paxton (SPIE, San Jose, CA, USA, 2000), pp. 222-233.
- ²⁰ V Daneu, A Sanchez, T Y Fan, H K Choi, G W Turner, and C C Cook, Optics Letters **25**, 405-407 (2000).
- ²¹ Clarkson, W. A. Clarkson, V Matera, A Abdolvand, TMJ Kendall, D. C. Hanna, J Nilsson, and PW Turner, in *Quantum Electronics and Photonics* (Glasgow, UK, 2001), p. 15.
- ²² Erik J. Bochove, Proceedings of SPIE **4270**, 95-104 (2001).
- ²³ Erik J. Bochove, in *Laser Resonators and Beam Control V*, edited by Alexis V. Kudryashov (SPIE, San Jose, CA, USA, 2002), pp. 31-38.
- ²⁴ S. J. Augst, A. K. Goyal, R. L. Aggarwal, T. Y. Fan, and A. Sanchez, Optics Letters **28**, 331 (2003).
- ²⁵ Steven C. Tidwell, Steve Roman, Don Jander, and Dennis D. Lowenthal, in *High-Power Diode Laser Technology and Applications*, edited by Mark S. Zediker (SPIE, San Jose, CA, USA, 2003), pp. 42-46.

- ²⁶ Anping Liu, Roy Mead, Tracy Vatter, Angus Henderson, and Ryan Stafford, in *Fiber Lasers: Technology, Systems, and Applications*, edited by L. N. Durvasula (SPIE, San Jose, Ca, USA, 2004), pp. 81-88.
- ²⁷ B. Chann, R. K. Huang, L. J. Missaggia, C. T. Harris, Z. L. Liau, A. K. Goyal, J. P. Donnelly, T. Y. Fan, A. Sanchez-Rubio, and G. W. Turner, *Optics Letters* **30**, 2104 (2005).
- ²⁸ Paul Salet, Gaëlle Lucas-Leclin, Gérard Roger, Patrick Georges, Philippe Bousselet, Christian Simonneau, Dominique Bayart, Nicolas Michel, Sophie-Charlotte Auzanneau, M. Calligaro, O. Parillaud, M. Lecomte, and Michel Krakowski, in *Advanced Solid-State Photonics* (Optical Society of America, 2005), p. MF32.
- ²⁹ T. Y. Fan and A. Sanchez, in *Fiber Lasers II: Technology, Systems, and Applications*, edited by L. N. Durvasula, Andrew J. W. Brown, and Johan Nilsson (SPIE, San Jose, CA, USA, 2005), pp. 157-164.
- ³⁰ Andreas Jechow, Volker Raab, and Ralf Menzel, *Applied Optics* **45**, 3545 (2006).
- ³¹ Ole Bjarlin Jensen, Birgitte Thestrup, Peter Eskil Andersen, and Paul Michael Petersen, *Applied Physics B Lasers and Optics* **83**, 225-228 (2006).
- ³² Anping Liu, in *Proceedings of SPIE* (Spie, 2006), pp. 621307-621307-9.
- ³³ Thomas H. Loftus, Anping Liu, Paul R. Hoffman, Alison M. Thomas, Marc Norsen, Rob Royse, and Eric Honea, *Optics Letters* **32**, 349 (2007).
- ³⁴ Sandro Klingebiel, Fabian Röser, Bülel Ortac, Jens Limpert, and Andreas Tünnermann, *Journal of the Optical Society of America B* **24**, 1716 (2007).
- ³⁵ Steven J. Augst, Jinendra K. Ranka, T. Y. Fan, and Antonio Sanchez, *Journal of the Optical Society of America B* **24**, 1707 (2007).
- ³⁶ Pratheepan Madasamy, Tom Loftus, Alison Thomas, Pat Jones, and Eric Honea, in *Proceedings of SPIE* (Spie, 2008), pp. 695207-695207-10.
- ³⁷ Steven J. Augst, Ryan C. Lawrence, T Y. Fan, Daniel V. Murphy, and Antonio Sanchez, in *Frontiers in Optics* (Optical Society of America, 2008), p. FWG2.
- ³⁸ O. Schmidt, C. Wirth, I. Tsybin, T. Schreiber, R. Eberhardt, J. Limpert, and A. Tünnermann, *Optics Letters* **34**, 1567 (2009).

- ³⁹ C. Wirth, O. Schmidt, I. Tsybin, T. Schreiber, T. Peschel, F. Brückner, T. Clausnitzer, J. Limpert, R. Eberhardt, A. Tünnermann, M. Gowin, E. ten Have, K. Ludewigt, and M. Jung, *Optics Express* **17**, 1178 (2009).
- ⁴⁰ Deepak Vijayakumar, Ole B. Jensen, and Birgitte Thestrup, *Optics Express* **17**, 5684 (2009).
- ⁴¹ Yunxia Li, Qiaoli Li, Shengbao Zhan, Wen Meng, and Shanghong Zhao, in *2009 International Conference on Optical Instruments and Technology: Optoelectronic Imaging and Process Technology*, edited by Toru Yoshizawa, Ping Wei, and Jesse Zheng (SPIE, Shanghai, China, 2009), p. 75132R-7.
- ⁴² Chr. Wirth, O Schmidt, I Tsybin, Thomas Schreiber, S Böhme, T Peschel, T Clausnitzer, F Röser, J Limpert, R Eberhardt, and A Tünnermann, in *Advanced Solid-State Photonics* (Optical Society of America, 2009), p. TuB14.
- ⁴³ Oliver Schmidt, Thomas V. Andersen, Jens Limpert, and Andreas Tünnermann, in *Advanced Solid-State Photonics* (Optical Society of America, 2009), p. TuA4.
- ⁴⁴ S. Hugger, F. Fuchs, Rolf Aidam, W. Bronner, R. Loesch, Q. Yang, N. Schulz, J. Wagner, E. Romasew, M. Raab, and H. D. Tholl, in *Laser Technology for Defense and Security V*, edited by Mark Dubinskii and Stephen G. Post (SPIE, Orlando, FL, USA, 2009), p. 73250H-7.
- ⁴⁵ Benjamin G. Lee, Jan Kinsky, Anish K. Goyal, Christian Pflugl, Laurent Diehl, Mikhail A. Belkin, Antonio Sanchez, and Federico Capasso, in *Lidar Remote Sensing for Environmental Monitoring X*, edited by Upendra N. Singh (SPIE, San Diego, CA, USA, 2009), pp. 746004-9.
- ⁴⁶ Deepak Vijayakumar, Ole Bjarlin Jensen, Ralf Ostendorf, Thomas Westphalen, and Birgitte Thestrup, *Optics Express* **18**, 893 (2010).
- ⁴⁷ F. Röser, S. Klingebiel, A. Liem, T. Schreiber, S. Höfer, J. Limpert, T. Peschel, R. Eberhardt, and A. Tünnermann, *Proceedings of SPIE, the International Society for Optical Engineering* 61020T.1-61020T.6 (2006).
- ⁴⁸ Igor V. Ciapurin, *Proceedings of SPIE* **4974**, 209-219 (2003).
- ⁴⁹ Igor Ciapurin, Vadim Smirnov, and Leonid Glebov, in *Solid State and Diode Laser Technology Review* (2004), pp. 4-7.

- ⁵⁰ Igor V. Ciapurin, *Proceedings of SPIE* **5742**, 183-194 (2005).
- ⁵¹ Armen Sevian, in *Proceedings of SPIE* (Spie, 2006), p. 62160V-62160V-12.
- ⁵² Oleksiy Andrusyak, Igor Ciapurin, Vasile Rotar, Armen Sevian, George Venus, and Leonid Glebov, in *Solid State and Diode Laser Technology Review* (2006), pp. 2-7.
- ⁵³ Oleksiy Andrusyak, Igor Ciapurin, Vadim Smirnov, George Venus, and Leonid Glebov, in *Proceedings of SPIE* (Spie, 2007), p. 64531L-64531L-7.
- ⁵⁴ Oleksiy Andrusyak, Igor Ciapurin, Armen Sevian, Vadim Smirnov, George Venus, and Leonid Glebov, in *Conference on Lasers and Electro-Optics/Quantum Electronics and Laser Science Conference and Photonic Applications Systems Technologies* (Optical Society of America, 2007), p. JTuA85.
- ⁵⁵ Armen Sevian, Oleksiy Andrusyak, Igor Ciapurin, Vadim Smirnov, George Venus, and Leonid Glebov, *Optics Letters* **33**, 384-386 (2008).
- ⁵⁶ Oleksiy Andrusyak, Igor Ciapurin, Vadim Smirnov, George Venus, Nikolai Vorobiev, and Leonid Glebov, in *Fiber Lasers V: Technology, Systems, and Applications*, edited by Jes Broeng and Clifford Headley III (SPIE, San Jose, CA, USA, 2008), pp. 687314-8.
- ⁵⁷ Oleksiy Andrusyak, Vadim Smirnov, George Venus, and Leonid Glebov, in *Frontiers in Optics* (Optical Society of America, 2008), p. FWG3.
- ⁵⁸ X Chu, S Zhao, L Shi, S Zhan, J Xu, and Z Wu, *Optics Communications* **281**, 4099-4102 (2008).
- ⁵⁹ Andrusyak, Drachenberg, Venus, Smirnov, and Glebov, in *Solid State and Diode Laser Technology Review* (2008), pp. 3-7.
- ⁶⁰ Oleksiy Andrusyak, Vadim Smirnov, George Venus, Nikolai Vorobiev, and Leonid Glebov, in *Proceedings of SPIE* (Spie, 2009), p. 71951Q-71951Q-11.
- ⁶¹ Oleksiy Andrusyak, Vadim Smirnov, George Venus, and Leonid Glebov, *Optics Communications* **282**, 2560-2563 (2009).
- ⁶² Oleksiy Andrusyak, PhD Dissertation, University of Central Florida (2009).

- ⁶³ G. B. Ingersoll and J. R. Leger, in *Fiber Lasers VI: Technology, Systems, and Applications*, edited by Denis V. Gapontsev, Dahv A. Kliner, Jay W. Dawson, and Kanishka Tankala (SPIE, San Jose, CA, USA, 2009), p. 71951P-12.
- ⁶⁴ Derrek R. Drachenberg, Oleksiy Andrusyak, Ion Cohanoschi, Ivan Divliansky, Oleksiy Mokhun, Alexei Podvyaznyy, Vadim Smirnov, George B. Venus, and Leonid B. Glebov, in *Fiber Lasers VII: Technology, Systems, and Applications*, edited by Kanishka Tankala (SPIE, San Francisco, California, USA, 2010), p. 75801U-9.
- ⁶⁵ Zhan Sheng-bao, Zhao Shang-hong, Chu Xing-chun, Wu Zhuo-liang, and Shi Lei, *Optics & Laser Technology* **42**, 308-312 (2010).
- ⁶⁶ C.R. Doerr, C.H. Joyner, and L.W. Stulz, *IEEE Photonics Technology Letters* **11**, 635-637 (1999).
- ⁶⁷ A. S. Arnold, J. S. Wilson, and M. G. Boshier, *Review of Scientific Instruments* **69**, 1236 (1998).
- ⁶⁸ J Bjorkholm, T Damen, and J Shah, *Optics Communications* **4**, 283-284 (1971).
- ⁶⁹ M. Fleming and A. Mooradian, *Quantum Electronics, IEEE Journal Of* **17**, 44-59 (1981).
- ⁷⁰ C J Hawthorn, K P Weber, and R E Scholten, *Review of Scientific Instruments* **72**, 4477-4479 (2001).
- ⁷¹ Haim Lotem, *Applied Optics* **33**, 930-934 (1994).
- ⁷² O Schmidt, C Wirth, D Nodop, J Limpert, T Schreiber, T Peschel, R Eberhardt, and A Tünnermann, *Optics Express* **17**, 22974-82 (2009).
- ⁷³ Herwig Kogelnik, *The Bell System Technical Journal* **48**, 2909-2947 (1969).
- ⁷⁴ Igor V. Ciapurin, Leonid B. Glebov, and Vadim I. Smirnov, *Optical Engineering* **45**, 015802-9 (2006).
- ⁷⁵ Leonid B. Glebov, Julien Lumeau, Sergiy Mokhov, Vadim Smirnov, and Boris Ya. Zeldovich, *Journal of the Optical Society of America A* **25**, 751 (2008).
- ⁷⁶ Leonid B. Glebov, in *Conference on Lasers and Electro-Optics* (Optical Society of America, 2010), p. CThX1.

- ⁷⁷ Derrek Drachenberg, Ivan Divliansky, Vadim Smirnov, George Venus, and Leonid Glebov, in *Proceedings of SPIE*, edited by Jay W. Dawson (SPIE, 2011), pp. 7914-79141F-1.
- ⁷⁸ S Mokhov, D Drachenberg, G Venus, B Zeldovich, and L Glebov, in *APS March Meeting* (2011), p. Presentation.
- ⁷⁹ Derrek Drachenberg, Ivan Divliansky, Vadim Smirnov, George Venus, and Leonid Glebov, in *2011 Conference on Lasers and Electro-Optics Europe and 12th European Quantum Electronics Conference (CLEO EUROPE/EQEC)* (IEEE, 2011), pp. 1-1.
- ⁸⁰ Mokhov, in *Proceedings of SPIE*, edited by Stephen Davis, Michael Heaven, and Thomas Schreimphf (San Francisco, California, USA, 2011), pp. 7915-17 (presentation).